The Conversion of Pyridine Molecule up to Hetero carbon Nanomaterial by Solution Plasma

Kyusung KIM

The Conversion of Pyridine Molecule up to Hetero carbon Nanomaterial by Solution Plasma

A Doctoral Dissertation by

Kyusung KIM

2020

Graduate School of Engineering,

Department of Material Science and Engineering,

Nagoya University

List of contents

Chapter 1

Introduction

Chapter 1 – Introduction

1. 1. Hetero carbon nanomaterial and conventional synthesis method

1. 1. 1 Hetero carbon nanomaterial

Carbon has isomers from zero dimensions to three dimensions. The diverse bonding structures of carbon atoms are caused varying properties of carbon material. Due to this reason, the carbon materials always have large attentions not only in research area also industrial fields for a long time. Various kinds of carbon materials have been used for several applications, from conventional types (graphite, diamond, activated carbon) and to recent nano-scaled type (carbon nanotubes, graphene, carbon dot, graphene ribbons). The carbon nanomaterials take a unique place in nano science for their exceptional thermal, mechanical, chemical and electrical properties, and then have been developed for advanced applications in areas as diverse as energy storage and conversion, gas storage, smart sensors, targeted drug delivery, catalyst support, field-emission devices, quantum wires, and nano electronics. [1-3]

To modify the performance of carbon materials, many researchers have an effort to synthesize hetero carbon nanomaterials by doping various kinds of hetero atoms, recently. The hetero atoms in the carbon structures give the polarizes neighboring carbon atoms, as a result, produce an imbalance charge in the carbon structure. Therefore, carbon nanomaterials with hetero atoms, such as nitrogen(N) [4-6], boron (B) [7,8] , phosphorus (P) [9], sulfur (S) [10] have attracted tremendous attention. As doping nitrogen atoms into graphene structure, the several properties of N-graphene quite change compared with the pure graphene. For example, the charge distribution of carbon atoms have been changed to relative positive by an effect of the neighbor nitrogen atoms which has relative negative charge [11], it induces the activate

reaction area on the surface of graphene. This activated reaction part can conduct an oxygen reduction as catalytic reactions efficiently. Also, it was confirmed by theoretical calculation that doped hetero atoms in the carbon sheet structure to modulate the surface electronic structure plays an important role in the catalytic performance [12].

1. 1. 2 Conventional synthesis method

1) Chemical vapor deposition (CVD) method

Chemical vapor deposition is a popular the synthesis method recently to prepare carbon nanosheets [13], carbon nanofiber [14], graphene [15], N-doped graphene [16]. For fabricating the N-doped graphene, nitrogen containing gas is mixed into a hydrogen carbon source gas employed with the metal substrate for catalyst in a high temperature. After segregation of the precursors and they recombine into N-doped graphene [17-18]. The nitrogen containing organic solvent also used as precursor to obtain N doped graphene. However, it is required t o consider the type of N containing molecule. Because, the pyridine can form N dop ed graphene owing to their bonding energy while the acrylonitrile is difficult to synth esize by effect of C≡N triple bond [19]. Furthermore, the level of nitrogen containing can be large influenced to N doped graphene. When the NH_3/ CH_4 ratio increased from 25 to 50 %, the N contents in graphene changed from 3.2 up to 8.9 at. % [20].

2) Arc-discharge method

The method can produce pristine or N doped CNTs using the evaporation the carbon source as graphite [22], also nitrogen-doped graphene (NG) was synthesized using hydrogen gas with pyridine or ammonia gas [23]. The N doped graphene size which prepared by this method is below 1 μm

3) Segregation growth method

This approach has an advantage to make large scale of product and uniform contents. In this process, boron layer with nitrogen and nickel layers with carbon are deposited on the substrate using electron beam evaporation. And then, the carbon atoms will segregate out from the nickel layer with trapping of boron atoms by nickel layer during the vacuum annealing step. At last, combination reaction of carbon and nitrogen atoms [24]. The concentration of nitrogen in N doped graphene can be controlled by the deposited layers thickness up to 2.9 %.

4) Solvothermal method

The solvothermal method was favorable for synthesis of large amount production [25]. The N doped graphene quantum dots (NGQDs) were successfully fabricated by solvothermal method with organic solvent with nitrogen as dimethylformamide was reported. Generally, the performance of GQD is not enough as compared with semiconductor QDs. However, it acquire the high value after doped N in carbon-based nanomaterials.

5) Thermal treatment method

The N doped graphene can be obtained from exfoliation of graphite oxide in the nitrogen gas atmosphere with thermal treatment at 1050 °C [26]. But, their nitrogen content in the N doped graphene is quite low. Other type of thermal treatment, electrical annealing, synthesize graphene nano ribbon (GNR) with nitrogen [27]. The N-GNR can be obtained from N-graphene sheet with NH_3 gas atmosphere.

6) Hydrazine hydrate (N_2H_4) Method

Using the NH_3 solution with hydrazine, reduction of graphene oxide (GO) produce the N doped graphene [28]. When the reduction temperature is 80 °C, the nitrogen concentration in N-graphene is around 5 %. The reduction temperature is important to control of N contents,

because the N contents decreased by desorption of hydrazine in high temperature. The temperature also affect to the morphology of N doped graphene. For instance, the sheet type of N doped graphene was formed in the low temperature (under 120°C), but the obvious aggregation in N doped carbon was observed at the higher temperature.

7) Plasma Treatment method

The carbon atoms were partially substituted by nitrogen atoms in carbon nano tubes structure with nitrogen plasma treatment [29-30]. Also, in the case of graphene, a doping of nitrogen atom was reported by exposing graphene to nitrogen plasma with same mechanism in the case of CNT. The exposure time and power of plasma controlled the contents of nitrogen from 3 to 8.5 at. % [31].

1. 2. Solution plasma

1.2.1 Fundamental of solution plasma

Solution plasma generated in the solution when high voltage applied. It is non-equil ibrium plasma since the electron temperature is much higher (T_e ~10^4 K) that that of ion or neutrons (T_i, T_n ~300 K). Thus, the thermal effect of heavy particles can be i gnored [32]. This reason is how to keep the working temperature of the solution near the room temperature. During the plasma generated in the solution, various kinds of reactive species occurred, such as radicals, electrons, ions. Using the unique reaction, nano-scaled materials can be synthesized rapidly without limitation of types of resourc e. The metal or metal oxide nanoparticle were synthesized by sputtering of metal elec trode or reduction of metal ion from aqueous solution with salts [33-35]. A synthesis of carbon material from organic solvents as benzene were also reported [36]. Further more, nanocomposite material of metal nanoparticle supported on the carbon material

was revealed [37, 38].

1.2.2 Experimental set up of solution plasma

The configuration of solution plasma is presented in figure 1.1. The reactor include s electrodes, silicon plug, ceramic tubes and a bipolar power supply. The detailed info rmation of three important parts (reactor, electrodes, bipolar pulse power supply) are d escried as follows:

1) Reactor

The reactor should be selected by size and type of material. In general, the hea t and impact resisting glass were applied for containing various kinds of solvents. In this study, 100 mL volume of glass beaker was used.

2) Electrodes

Electrodes can be picked among the various kinds of material rely for the purp ose of the experiments. For instance, a metal electrode such as tungsten, nickel, ir on, zinc, platinum can be used for synthesis the metal nano particles. The graphite electrode also employed to make carbon material. Among the various types of el ectrodes, tungsten electrodes commonly used due to their excellent stability. In ord er to concentrate energy between a gap of electrodes, electrodes should be covered using ceramic tube.

3) Bipolar pulse power supply

The bipolar pulse within the microsecond range pulse could prevent an instantan eous large energy supply into plasma system with the excitation of only electrons except ions. Therefore, the plasma can be kept stable in the range of non-thermal

plasma. The applied voltage (~ 4kV), frequency (~200kHz) and pulse width (~4.0 μs) are controllable parameters in this power supply. The parameter can influence to characteristic of material synthesized by solution plasma.

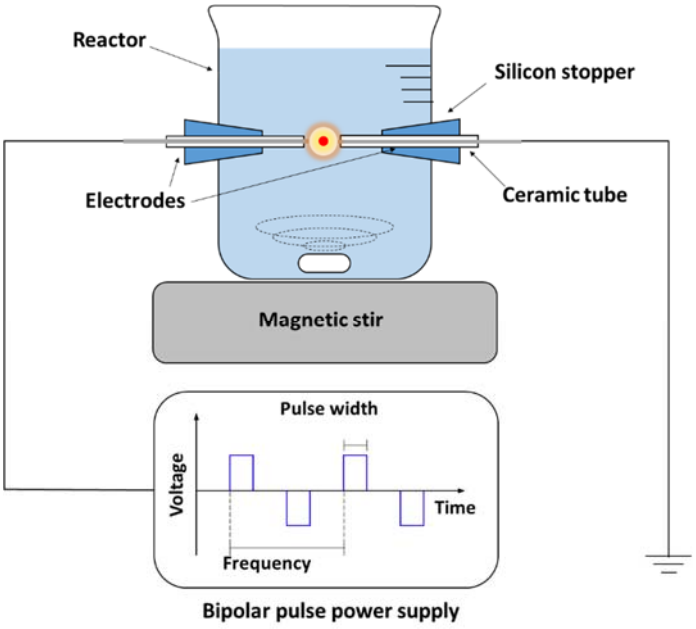

Figure 1.1 Schematic of solution plasma experimental set up

1.2.3 Advantage of solution plasma to synthesize hetero carbon nanomaterial

Especially, the SP method has been focused on a fabrication of hetero carbon nano materials. As mentioned before, in the high temperature of conventional synthesis met hod, a doping the nitrogen atoms in the carbon framework is quite difficult procedure.

As the results, the contents of hetero atoms in the carbon material synthesized by conventional method are under 5 at.%. However, the hetero graphene fabricated by the SP showed 13% of nitrogen contents using EMIM-DCA and DMF [39]. The high nitrogen concentration was attributed to the mechanism of synthesis carbon by the SP. During the SP for synthesizing carbon material, a glow discharge generated in the organic solvent and many kinds of species from the organic monomer such as C_2, CH, H radicals are observed in the plasma phase, representatively. During the discharge in hetero cyclic molecules, CN, OH radical can be formed from plasma phase. It was considered that restructuring of crystalline carbon structure is much difficulty using the radical from a dissociation of monomer. The other pathway for synthesis carbon by SP occurred at the interface between the plasma/liquid phases. The SP leads to redox reaction of molecules as catalysts at the interface. Due to this reaction, the organic monomer near the plasma phase convert to radical by electron transfer. The rapid fabrication of carbon from organic monomer by the SP was initiated by this mechanism. Through the mechanism, hetero cyclic molecules can be converted to hetero carbon nano material without a loss of hetero atom.

1. 3 Radical polymerization process

Formation of polymer using the radical species show the rapid synthesis rate due to the high reactivity of radicals. This process consist of three steps; i) initiation, ii) propagation, and iii) termination.

First, initiation is the first step of the polymerization of molecules. In this step, a reactive molecule which can start the polymerization is created. In this step, one or two radicals occur from the initiating molecules by several mechanism. As below, the various mechanism of a generating of radicals be introduced.

1) Thermal decomposition

A chemical decomposition of molecule by heat lead to formation of radicals. In this reaction, it is required heat energy to break chemical bonds. Therefore, quite large energy consume to reach the decomposition temperature.

2) Photolysis

The radiation by photo lead to a hemolytic cleave a molecule and then two radicals occurred. Photolysis is well known to cleave metal iodides or alkyls, and azo compounds usually. When the radical is in lowest triplet excited state, the photolysis also generated. The photolysis initiation required some condition such as high absorptivity for UV, solubility in the binder system.

3) Redox reactions

A reduction of hydrogen peroxide or an alkyl hydrogen peroxide by some metal ion lead to formation of hydroxyl radicals. Cr^{2+}, V^{2+}, Ti^{2+}, Co^{2+}, and Cu^{2+} ion also employed as redox agents.

4) Ionizing radiation

The free radical occurred by an ejection of electrons from the resource species by α-, β-, γ-, or x-rays. During this reaction, ionizing, radiation, ejection dissociation and electron capture occurred and they also lead to produce a radical.

5) Electrochemical

Electrolysis is generated by electron transfer between molecule and electrode. In the region of cathode, an anion radical is formed when the cathode offer an electron to monomer. Oppositely, a cation radical is formed by losing an electron at the anode. The radical ions can initiate free radical polymerization. This method is useful for polymer films coating on metal surfaces.

In the second, a propagation step, radicals propagate from the initiator molecules to neighboring monomer. The free radical formed by initiation can reaction with other molecule due to their high reactivity. In the case of an ethene molecule, two kind of bond presence between two carbon atoms. When the ethene react with free radical, the one electron in π bond can be used to make stable bond [40]. After that, the whole molecule convert to radical by other electron returns to the second carbon atom. These reactions are beginning state of radical polymerization.

Propagation is an intermediate step of radical polymerization process. The molecule reacted with free radical during the initiation step converted to free radical. Thus, it can be reaction continuously with the other molecules. Finally, in a termination step, the polymerization of molecules discontinues when the propagating radical react with other radical. The state of radial becomes stable by reaction with the initiator, other propagating radical or impurity. The figure 1.2 shows the typical radical polymerization process in three steps.

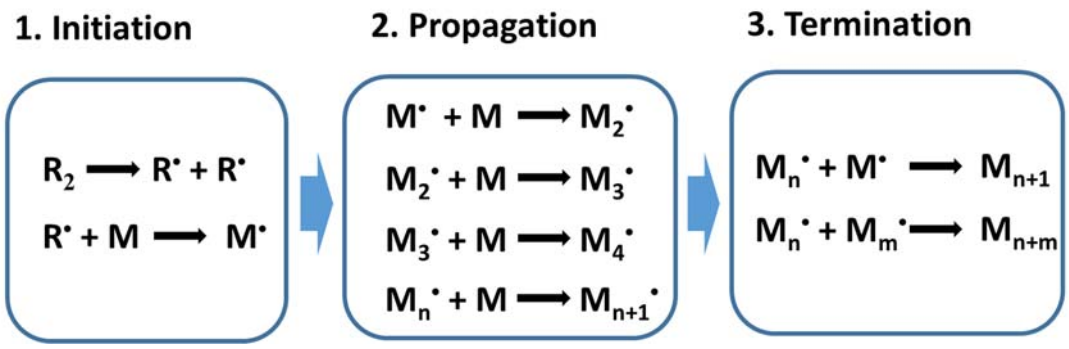

Figure 1.2 Step of radical polymerization process

1. 4. Carbon dots

1.4.1 Carbon dots

Recently, carbon dots (CDs), the new research subject of carbon nanoscience, is discovered. CDs are nanoparticles smaller than 10 nm and due to their small size, an important property is a tunable fluorescence in the visible range. The CDs are accompanied by some benefits as compared with conventional metal or semiconductor type quantum dots (QDs) as low cost and excellent biocompatibility. These advantages of CDs make them using in a quite broad range of applications without strong limitation, especially bio imaging and ion/molecule sensing [41-43].

However, the quantum yield, energy efficiency of absorbing light to emit light, is of CDs (10%) quite lower than QDs (60%). Thus, the research of CDs is still developed to solve the mentioned problem. Nano-scaled materials shows unique property due to the quantum confinement effect. The electrons loss leads to quantization on density of states is shown in figure 1.3. The fundamental of the electronic band states, the key factors to determine their fluorescence, and the relation between excitation and emission. Therefore, a much effort is in

progress to find the effective ways to control the electronic band structure. The effective method to tailor band gap of CDs is a doping the hetero atoms for generating new band. For instance, a nitrogen atom in the carbon structure which has lone pair electrons generate n band between pi-pi* bands.

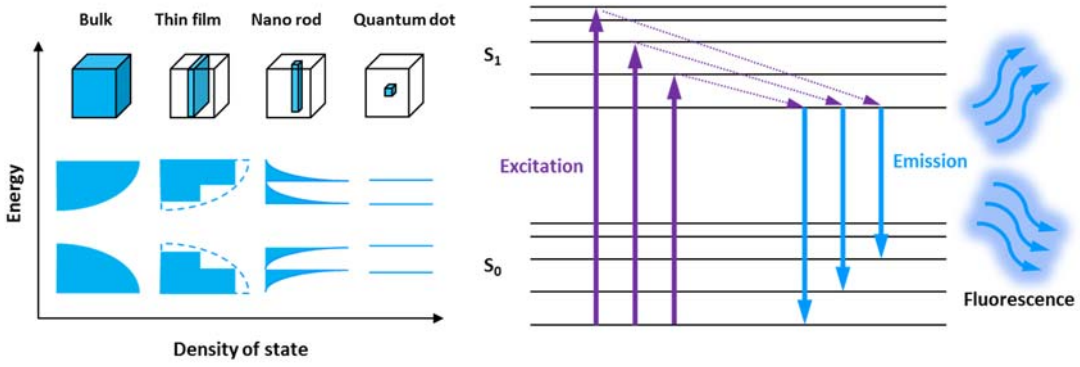

Figure 1.3 Quantum confinement effect and mechanism of fluorescence

1.4.2 Conventional method for synthesis of CDs

- Top-down method

An exfoliating the nano-scale particles from carbon materials, such as bulk graphite, few layer of graphene and activated carbon is carried out. The advantage of top-down methods is keeping sp^2 structures with high crystallinity, but their luminescent properties are quite low due to lack of doped hetero atoms. Thus, chemical modification of the surface of CDs enhance to increase the quantum yield.

1) Arc-discharge

When the arc discharge occurred on the surface of bulk carbon material, fluorescent carbon dots successfully synthesized. A fluorescent carbon dots can be separated from the soot. The quantum yield of the fluorescence was confirmed 1.6% at 366 nm of excitation wavelength

[44]. Its advantage is a simple, high purification, an environment-friendly methods. However, the low synthesis rate and difficulty of chemical modification is critical problem.

2) Laser ablation

Laser bean is employed to irradiate the surface of carbon material by a. The CDs were prepared using a Nd:YAG laser with argon carrier gas. Only a 10% of low quantum yield was achieved with surface passivation by the nitric acid CDs [45]. The result showed that this method requires several complex processes to get considerable photoluminescence properties.

3) Electrochemical synthesis

Electrochemical method to take carbon dot from graphite or carbon nanotubes is an attractive method due to the reasonable cost and high production rate. An electrochemical route to prepare the CDs in the acetonitrile solution [46]. The working electrode as MWCNT-based carbon sheet, coupling with Pt counter electrode and an $Ag/AgClO_4$ reference electrode is prepared to consist electrochemical system. The CDs with blue luminescence showed 6.4% of QY were obtained through the cycling voltage. Also, the products can be formed from graphite rod in aqueous solution by the electro oxidation [47]. However, a requirement of post treatment for changing the surface state to achieve high QY is a problem to solve.

- Bottom-up method

In the case of top-down synthesis, it is required a post-treatment to give the surface modification to pristine CDs to improve their performance. Oppositely, a bottom-up method can synthesize CDs with giving functional group. In general, hydrothermal, thermal combustion, microwave, ultrasonic was employed to fabricate CDs from small organic molecules under variable conditions.

4) Hydrothermal, thermal combustion methods

The advantages of hydrothermal methods for producing fluorescent CDs are environment friendly and economic method without high-technology equipment. Using Citric acid, glucose, chitosan, protein as precursor were reported in formation procedures of CDs by this reactions [48-51]. The first report of hydrothermal synthesis of CDs has reported in 2010 [52]. L-ascorbic acid mixed in water and ethanol solution were employed and the solution reacted in the autoclave at 180 C for 4 hr. The prepared CDs show the 7 % of quantum yield after dialysis process. Through thermal combustion, CDs also can be synthesized from various type of hydrocarbon resources [53-56]. Although the combustion method is a simple method, the quite low QY (below 3%) make a limitation to use.

5) Template-assisted methods

This method is suggested to avoid agglomeration of carbon particles. F127 as an amphiphilic triblock copolymer was used for surface modification of silica spheres. The F127/SiO_2 composites are successfully fabricated and it can be converted to carbon material with silica template. Finally, only fluorescent CDs were obtained by etching of the template using NaOH solution [57]. Size distribution and morphology can be controlled by this methods. For producing CDs, the mesoporous silica spheres as a template and N-hexadecyl amine and citric acid as the carbon precursors was employed [58]. The 2 nm of CDs were synthesize uniformly with blue emission and showed 23 % of quantum yield.

6) Microwave/ultrasonic-assisted method

The microwave method can synthesize CDs rapidly with high quantum yield rapid. But one of the disadvantage is a limitation of precursor selection. Polyethylene glycol (PEG) and saccharide solution was reacted 500 W of microwave for 10 min. [59]. Also, ultrasonic treatment was presented that a CDs preparation with active carbon in hydrogen peroxide solution [60]. The obtained CDs exhibited strong visible emission and excellent PL properties.

1. 5. Objective and outline of the thesis

For the demand of carbon nanomaterials for many applications, especially the requirement of the hetero carbon nanomaterial rises up. Because property of practical scaled pristine carbon nanomaterials difficult to satisfy as that of experimental scaled. Thus, the synthesis of hetero carbon material is focused for solving the problem. Various kinds of hetero atoms (B, N, P, S) in the carbon structure can use for an improvement of property. Among them, a nitrogen atom which has 5 valence electrons and similar size with carbon atom is a best candidate atom among various kinds of hetero-atoms. For instance, when a nitrogen atom is doped into graphene sheet, a charge distribution of graphene sheet occur due to effect of relative negative nitrogen dopants. At last, it leads to an improvement of electrical property effectively [20, 61]. In the case of catalyst effect for oxygen reduction reaction, the relative charge of carbon atoms changed to positive charge due to neighboring nitrogen atom which is favorable to react with oxygen molecules [62-64]. Also, the nitrogen atom in carbon quantum dots affects to the improvement of the quantum yield related to energy efficiency of light increased due to effects on the electronic band structure [65-67].

However, the fabrication of hetero carbon nanomaterial is not easy, in particular, high

concentration nitrogen doping is quite difficult by conventional methods. The reason might be a high temperature which could remove nitrogen atoms in the structure due to its light mass. So, volatilization of nitrogen and recrystallization of carbon structure occurs easily [17-19,24,26] (800-1300C°).

Therefore, in order to unzip the problem, exploring and developing of new synthesis method is needed. The solution plasma (SP) is an attractive alternative method for synthesis of nitrogen doped carbon material. During the synthesis, the SP method used the glow discharge in the solution, thus temperature of solution do not over the room temperature. And, the electron transfer occurs between plasma phase and hetero cyclic aromatic molecules in the liquid phase and it leads to polymerization of monomers by the C-H activation. Therefore, the solution plasma method is favorable to keep high contents of nitrogen in the carbon structure. Using these advantages, the previous studies reported that synthesis and analysis of nitrogen doped carbon nanomaterials from heterocyclic aromatic organic solvents such as pyridine, cyanopyridine, and imidazolium ionic liquid and they showed high concentration (13%) of nitrogen in the products [39].

However, the investigation of the formation process from the hetero organic molecule to the nitrogen doped carbon nanomaterials was not yet been clarified. Basically, the synthesis process from organic monomer for carbon is still unclear until now. The resonance-stabilized hydrocarbon-radical is suggested that it is starting reactant for fabricating of carbon material [68, 69]. The suggestion is similar to the pathway for carbon nanomaterial synthesis by solution plasma from benzene. During the solution plasma process, the organic molecules convert to radicals by plasma. By reaction with these radical, the carbon nanomaterial can be synthesized.

In contrast to symmetric pristine carbon structure, in the case of the nitrogen doped carbon

nanomaterial, the reaction part on heterocyclic molecule for synthesizing the nitrogen doped carbon is important. Because, N doped carbon showed different properties by not only concentration but also the position. The position of nitrogen in carbon structure decides the presence of lone pair electrons. Among the bonding configurations, the pyrrolic N doesn't have lone pair electrons, however, pyridinic N has a lone pair electrons. It leads to generate n band in electronic band structure, also affect to charge of neighboring carbon atoms. It means that same concentration of nitrogen make a different effect on nitrogen doped carbon nanomaterial. Therefore, a confirming of the position of nitrogen atom has a valuable meaning of the research fields and the investigation on the pathway of synthesis process would be a good way to predict the position of nitrogen. The heterocyclic molecules are converted by solution plasma and then the position of nitrogen in the synthesized intermediate products can be confirmed. Therefore, in this study, a conversion of the hetero cyclic aromatic molecule (pyridine) by SP was investigated for deep understanding how the hetero cyclic molecule change to hetero carbon nanomaterial the SP process.

In each chapter was introduced sequentially the conversion procedure of pyridine monomer by solution plasma.

In chapter 2, various kinds of products formed after 1, 5 second of solution plasma from pyridine were analyzed by GC-MS and their formation mechanism were discussed with the DFT calculation.

In chapter 3, the quantitative spectrochemical analysis were conducted using benzene, pyridine, and aniline during and after the solution plasma. The plasma phase and solution/solid phase were investigated, respectively.

In chapter 4, fluorescent carbon dots were synthesized and their optical properties were

discussed.

Finally, the summary of each chapter concluded in chapter 5.

Reference

1. Q. Zhang, J. Huang, W. Qian, T. Zhang, F. Wei, Small, 9, 1237, (2013)

2. L. Dai, D. Chang, J. Baek, W. Lu, Small, 8, 1130, (2012)

3. Z. Liu, X. Sun, N Nakayama, H. Dai, ACS Nano, 1, 50, (2007)

4. L. Qu, Y. Liu J. Back, L. Dai, ACS Nano, 4, 1321, (2010)

5. Y. Wang, Y. Shao, D. Matson, J. Li, Y. Lin, ACS Nano, 4, 1790, (2010)

6. D. Usachov, O. Vilkov, D. Haberer, D. Vyalikh, Nano Lett, 11, 5401 (2011)

7. S. Agnoli, M. Favaro, J. Mater. Chem. A, 4, 5002, (2016)

8. Z. Sheng, H. Gao, W. Bao, F. Wang, X. Xia, J. Mater. Chem., 22, 390, (2012)

9. C. Zhang, N. Mahmood, H. Yin, F. Liu, Y. Hou, Adv. Mater., 25, 4932, (2013)

10. Z. Ma, S. Dou, A. Shen, L. Tao, L. Dai, S. Wang, Angew. Chem. Int. Ed. Engl., 54, 1888 (2015)

11. H. Wang, T. Maiyalagan, X. Wang, ACS Catalysis, 2, 781, (2012)

12. W. Liang, J. Chen, Y. Liu, S. Chen, ACS Catalysis, 4. 4170, (2014)

13. J. Wang, M. Zhu, R. A. Outlaw, X. Zhao, D. M. Manos, B. C. Holloway, Carbon 42, 2867, (2004)

14. B. Boskovic, V. Stolojan, R. Khan, S. Haq, S. Ravi, P. Silva, Nature Materials 1, 165, (2002)

15. A. Reina, X. Jia, J. Ho, D. Nezich, H. Son, V. Bulovic, M. Dresselhaus, J. Kong, Nano Lett. 9, 30 (2009)

16. S. Maldonado, S. Morin, K. Stevenso, Carbon 44, 1429 (2006)

17. Qu L., Liu Y., Baek J. B., Dai L, ACS Nano 4, 1321 (2010)

18. Di C. A., Wei D., Yu G., Liu Y., Guo Y., Zhu D., Adv. Mater. 20, 3289 (2008)

19. Z. Lin, G. Waller, Y. Liu, M. Liu, C. Wong, Adv. Energy Mater. 2, 884 (2012)

20. Wei D., Liu Y., Wang Y., Zhang H., Huang L., Yu G, Nano Lett. 9, 1752 (2009)

22. R. Droppa, P. Hammer, A. Carvalho, M. Alvarez, Non-Cryst. Solids 874, 299 (2002)

23. L. Panchakarla, K. Subrahmanyam, S. Saha, A. Govindaraj, H. Krishnamurthy, U. Waghmare, C. Rao. Adv. Material 21 4726 (2009)

24. H.M. Jeong, J.W. Lee, W.H. Shin, Y.J. Choi, H.J. Shin, J.K. Kang, J.W. Cho, Nano Lett. 11, 2472 (2011)

25. M. Choucair, P. Thordarson, J. Stride, Nat. Nanotechnol 4, 30 (2009)

26. X. Li, D. Geng, Y. Zhang, X. Meng, R. Li, X. Sun, Electrochem. Comm. 13 822 (2011)
27. Wang X., Li X., Zhang L., Yoon Y., Weber P. K., Wang H., Guo J., Dai H., Science 324, 768 (2009)
28. Long, D., Li, W., Ling, L., Miyawaki, J., Mochida, I., Yoon, S. H., Langmuir 26, 16096 (2010)
29. Golberg, D., Bando, Y., Bourgeois, L., Kurashima, K., Sato, T., Carbon, 38, 2017. (2000)
30. Morant C., Andrey J., Prieto P., Mendiola D., Sanz J. M., Elizalde E., Phys. Status Solidi A 203, 1069 (2006)
31. Y. Shao, S. Zhang, M. Engelhard, G. Li, G. Shao, Y. Wang, J. Liu, A. Ilhan, Y. Lin, J. Mater. Chem., 20, 7491 (2010)
32. Nijdam, S, van Veldhuizen, E, Bruggeman P, Ebert U, Plasma Chemistry and Catalysis in gases and liquids 1 (2012)
33. N. Saito, J. Hieda, O. Takai, Thin Solid Film 518, 912 (2009)
34. G. Saito, S. Hosokai, M. Tsubota, T. Akiyama, J. Appl. Phys 110, 023302 (2011)
35. S. Kim, G. Kim, S. Lee, Mater. Lett. 62, 4354, (2008)
36. J. Kang, O. Li, N. Saito, Carbon, 60, 292 (2013)
37. J. Kang, O. Li, N. Saito, Nanoscale, 15, 6874 (2013)
38. G. Panomsuwan, S. Chiba, Y. Kaneko, N. Saito, J. Mater. Chem. A, 43, 18677 (2014)
39. S. Chae, G. Panomsuwam, M. Bratescu, K. Teshima, N. Saito. ACS Appl. Nano Mater. 2 1350 (2019)
40. P. Ehrlich, G.A. Mortimer, Adv. Polymer Sci. 7 386 (1970)
41. S. Sahu, B. Behera, T.K.Malti, S. Mohapatra, Chem. Comm. 70, 8835 (2012)
42. Y. Di, S. Guo, Nanoscale 8, 2532 (2016)
43. X. Sun, Y. Lei, Trends Anal. Chem. 89, 163 (2017)
44. A. Loukanov, R. Sekiya, M. Yoshikawa, N. Kobayashi, Y. Moriyasu and S. Nakabayashi, J. Phys. Chem. C, 120, 15867 (2016)
45. S. Zhu, Y. Song, X. Zhao, J. Shao, J. Zhang and B. Yang, Nano Res., 8, 355 (2015)
46. J. Zhou, C. Booker, R. Li, X. Zhou, T.-K. Sham, X. Sun and Z. Ding, J. Am. Chem. Soc., 129, 744 (2007)
47 S. Zhu, Q. Meng, L. Wang, J. Zhang, Y. Song, H. Jin, K. Zhang, H. Sun, H. Wang and B. Yang, Angew. Chem., Int. Ed. Engl., 52, 3953 (2013)

48. Q. L. Zhao, Z. L. Zhang, B. H. Huang, J. Peng, M. Zhang and D. W. Pang, Chem. Commun., 41, 5116. (2008)

49. Z. Yang, M. Wang, A. M. Yong, S. Y. Wong, X.-H. Zhang, H. Tan, A. Y. Chang, X. Li and J. Wang, Chem. Commun., 47, 11615 (2011)

50. Z. Zhang, J. Hao, J. Zhang, B. Zhang and J. Tang, RSC Adv., 2, 8599 (2012)

51. Y. Yang, J. Cui, M. Zheng, C. Hu, S. Tan, Y. Xiao, Q. Yang and Y. Liu, Chem. Commun., 48, 380 (2012)

52. B. Zhang, C.-Y. Liu and Y. Liu, Eur. J. Inorg. Chem., 28, 4411 (2010)

53. S. C. Ray, A. Saha, N. R. Jana and R. Sarkar, J. Phys. Chem. C, 113, 18546 (2009)

54. L. Tian, D. Ghosh, W. Chen, S. Pradhan, X. Chang and S. Chen, Chem. Mater., 21, 2803 (2009)

55. J. C. Vinci and L. A. Colon, Anal. Chem., 84, 1178 (2012)

56. Y. Li, L. Xu, T. Chen, X. Liu, Z. Xu and H. Zhang, Anal. Chim. Acta, 726, 102 (2012)

57. R. Liu, D. Wu, S. Liu, K. Koynov, W. Knoll and Q. Li, Angew. Chem., Int. Ed. Engl., 121, 4668 (2009)

58. J. Zong, Y. Zhu, X. Yang, J. Shen and C. Li, Chem. Commun., 47, 764 (2011)

59. H. Zhu, X. Wang, Y. Li, Z. Wang, F. Yang and X. Yang, Chem. Commun., 34, 5118. (2009)

60. H. Li, X. He, Y. Liu, H. Yu, Z. Kang and S.-T. Lee, Mater. Res. Bull., 46, 147 (2011)

61. Y. Qiu, X. Zhang, S. Yang, Phys. Chem. Chem. Phys., 13, 12554 (2011)

62. G. Ferrero, A. Fuertes, M. Sevilla, M. Titirici, Carbon, 106, 179 (2016)

63. D. Guo, R. Shibuya, C. Akiba, S. Saji, T. Kondo, J. Nakamura, Science, 22, 361 (2016)

64. J. Zhang, L. Dai, ACS Catal. 5, 7244 (2015)

65. Y. Zhang, D. Ma, Y. Zhuang, X. Zhang, W. Chen, L. Hong, Q. Yan, K. Yu, S. Huang, J. Mater. Chem. 22, 16714, (2012)

66. Z. Yang, M. Xu, Y. Liu, F. He, F. Gao, Y. Su, H. Wei, Y. Zhang, Nanoscale, 6, 1890 (2014)

67. Y. Zhang, D. Ma, Y. Zhang, W. Chen, S. Huang, Nano Energy, 2, 544 (2013)

68. K. Johansson, M. Gordon, P. Schrader, K. Wilson, H. Michelsen, Science, 361, 997 (2018)

69. M. Thomson, T. Mitra, Science, 361, 978, (2018)

Chapter. 2

The Initial Reactions from Pyridine to Hetero-Carbon Nanomaterials through Solution Plasma

Chapter. 2

The Initial Reactions from Pyridine to Hetero-Carbon Nanomaterials through Solution Plasma

2. 1. Introduction

Recently, hetero carbon nanomaterials doped which is doped hetero atoms (B or N) have been received a significant attention because of their potential as catalysts and field effect transistors [1-3]. However, the synthesis of hetero-carbon nanomaterials required high temperature (500-750°C) and long processing time [4-6]. Due to these kinds of problems, solution plasma (SP) process could be one of an alternative for the synthesis of carbon nanomaterials [7-9]. The SP is one of the non-equilibrium plasma type generated into a liquid and make unique reactions at the interface of the liquid/plasma phases [10, 11]. Using this reaction, the carbon nanomaterials can be synthesized from organic solvents. Especially, the strong advantage of SP methods for synthesizing hetero-carbon nanomaterials is that generating in the room temperature with atmospheric pressure. Oppositely, by pyrolysis which is represented conventional method, the hetero atoms are difficult to be contained in the carbon structure due to the breaking bonds at high temperatures. However, SP method might lead to polymerization of the organic monomers at room temperature. Thus the obtained products can be expected to contain a high amount of hetero-atoms. Using SP method, hetero-carbon nanomaterials could be synthesized from heterocyclic aromatic organic solvents such as pyridine, cyanopyridine, and pyrazine [12-14]. Although many studies about the

characteristics and application properties of the hetero-carbon nanomaterials [7-9, 12, 13] synthesized by SP had been done, the investigation on the synthesis process from the solvent to the hetero-carbon nanomaterials was not yet been clarified. The investigation of the products formed by the initial reaction of the organic solvent molecule after SP could help to understand the SP process. Therefore, in this research, a gas chromatography-mass spectrometry (GC-MS) was conducted for identifying of newly formed molecules. A coherent anti-stokes Raman spectroscopy (CARS) was employed to confirm the change of pyridine molecules by SP. Pyridine is suitable to be analyzed by Raman spectroscopy due to its high symmetry, and CARS is suitable for the detection of the changes in the liquid state of the molecule. The magnitude of CARS signal is stronger than that of the conventional Raman in liquids [15]. In order to detect generated radicals in the plasma, optical emission spectroscopy (OES) measurement was used. The partial charge of the molecule, total molecular energy change were performed by density functional theory (DFT) calculation.

2. 2. Experimental Details

2. 2. 1. SP method

Plasma discharged in 7 mL pyridine (with a purity higher than 99.5%, Kanto Chemical Co., Inc.) by bipolar power supply (Kurita) between 0.4 mm diameter of tungsten electrodes (Nilaco) covered with insulating ceramic tubes (Nilaco). The position of electrodes were centered at the reactor and their gap distance was kept at 0.5 mm. The pulse width was 1.0 μs and frequency was 20 kHz in the input energy.

2. 2. 2 Computational method

The molecular calculations were carried out using DFT calculation. Gaussian09 software package was used for the calculation of the partial charge, total energies, Raman wavenumbers, and Raman activity [16]. The basis sets of calculation was used UB3LYP hybrid functional and 6-311+G(2df,2p).

2. 2. 3. Characterization

GC-MS (JEOL, JMS-Q1050GC) measurement was performed to confirm newly formed molecules type after SP. In the column (HP-5, Agilent Technologies 19091J-413), He carrier gas was employed with 1.4 mL/min of flow rate. The temperature of column increased up to 250 °C with an increating rate of 10 °C/min. Also, mass spectrometry was carried out in the range of 20 to 600 m/z. 2 μL of samples were syringed using pulsed splitless injection mode. In the OES measurement, an optical fiber (P400-2-UV/Vis, Ocean Optics) connected to a spectrometer (Ocean Optics Inc., USB4000) was used. The mearusement distance from the optical fiber to the plasma area was fixed at 5 mm. The emission spectra were recorded from 300 to 800 nm of wavelength and its integration time is 0.01 sec and 3 averaged times. In the case of Raman spectra measurement for pyridine, CARS system (Tokyo Instruments, CO., Ltd.) was used as shown in Fig. 2.1. The laser radiation with 355 nm wavelength was generated by a neodymium doped yttrium aluminum garnet (Nd:YAG) crystal. The value of repetition frequency and pulse width of the laser were fixed at 10 Hz and 6 ns, respectively. Nd:YAG laser goes through two optical parametric oscillator crystals (OPO). In order to control Stokes radiation, the OPO_1 laser was conducted in the range from 500 to 600 nm, and the OPO_2 laser

as pump laser was fixed at 488 nm of wavelength. An intensified charge coupled device (iCCD) detector (Andor technologies) was carried out with 600 traces/mm of diffraction grating [17]. The CARS signal was scanned from 1010 to 970 cm^{-1} with 0.5 cm^{-1} step. The exposure time and accumulation were 0.5 sec and 10 times, respectively.

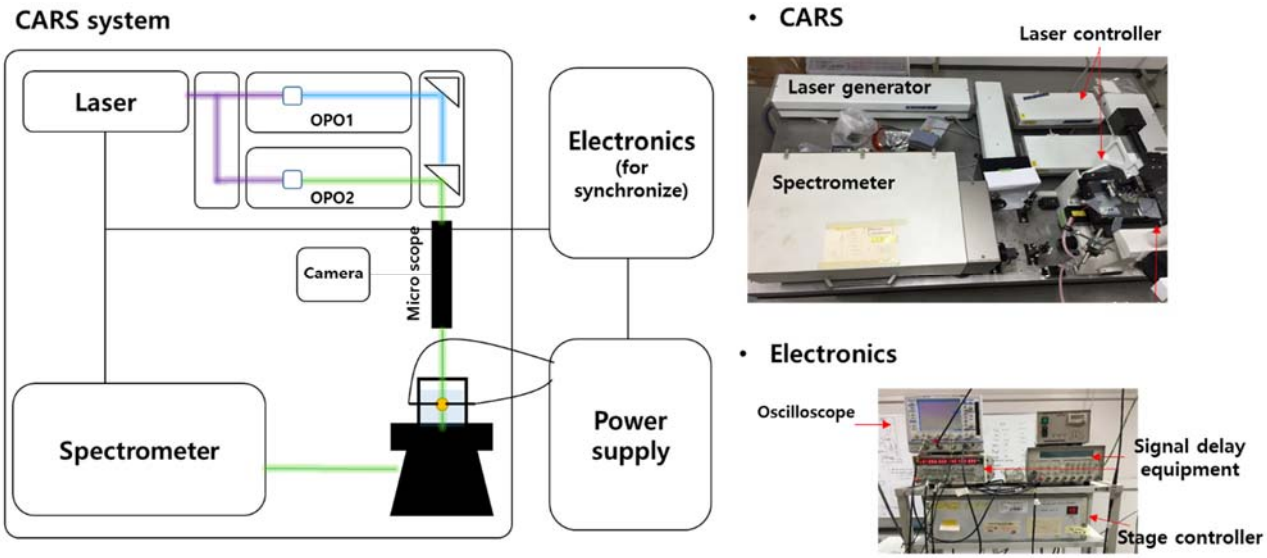

Figure 2.1 Experimental set up of CARS system

2. 3. Results and Discussion

To identify the initial reaction products formed after SP from pyridine, the solutions processed 1 and 5 sec were analyzed by GC-MS. Fig. 2.2 a) shows the analysis results of the molecules produced after different durations of the SP. In the GC-MS results, five types of molecules were dominantly observed (1) 4-cyanopyridine (MW:104), (2) 2-cyanopyridine (MW:104) (3) 2,2'-bipyridine (MW:156), (4) 2,4-bipyridine (MW:156), and (5) O-phenanthroline (MW:180) respectively. Also, (6) terpyridine (MW:233) was observed after SP 5 sec as given at Fig. 2.2 b).

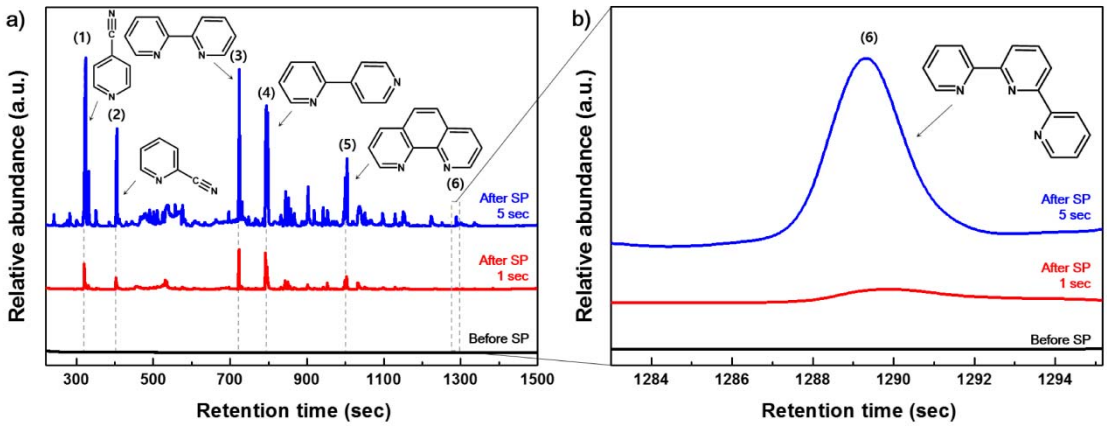

Figure 2.2 a), b) GC-MS analysis results of the pyridine before and after 1 and 5 sec ((1) 4-cyanopyridine, (2) 2-cyanopyirdine, (3) 2,2'-bipyridine, (4) 2,4'-bipyridine, (5) o- phenanthroline, (6) terpyridine).

The reaction path for the synthesis of molecules could be explained when the reactants and products are confirmed. Also, it is considered that the radical reaction is the dominant reaction pathway in the SP system. In the first step, the radical species are initially formed by plasma. In the next step, these radicals react with neighboring molecules, as a result, new free

radicals is formed. Also these new free radicals could make free radicals continuously by same mechanism. The final step consists in that two free radical species react with each other into a formation of new kind of molecule. Thus, in this study, the reaction pathway from pyridine to products by SP is explained by radical reaction. Fig. 2.3 shows the reaction way of the cyanopyridine molecules. In the case of cyanopyridine molecule, the CN radicals were generated by dissociation of pyridine molecule due to the plasma in the first step. The radical species produced from pyridine were observed by in situ OES, as shown in Fig. 2.4 [18, 19]. The emission bands associated with the CN system (transition $B^2\Sigma^+ \rightarrow X^2\Sigma^+$) were observed at the wavelengths in the range of 350 - 420 nm [20, 21]. The emission of diatomic carbon molecules (C_2) corresponding to the Swan bands are the transition from $d^3\Pi_g$ to $a^3\Pi_u$ in the range of 430 to 630 nm [21, 22]. The emission at 656 nm is associated to Balmer atomic hydrogen (H_α) [23]. The CN radical could react with the stable pyridine molecule by radical-nucleophilic aromatic substitution. In this reaction, the CN radical was nucleophile, so it could attack ortho or para position which is the electropositive (δ^+) position in pyridine molecule [24]. This reaction finished when the new radical formed by CN radical and pyridine molecule reacted with H radical, and then the stable cyanopyridine molecule is formed.

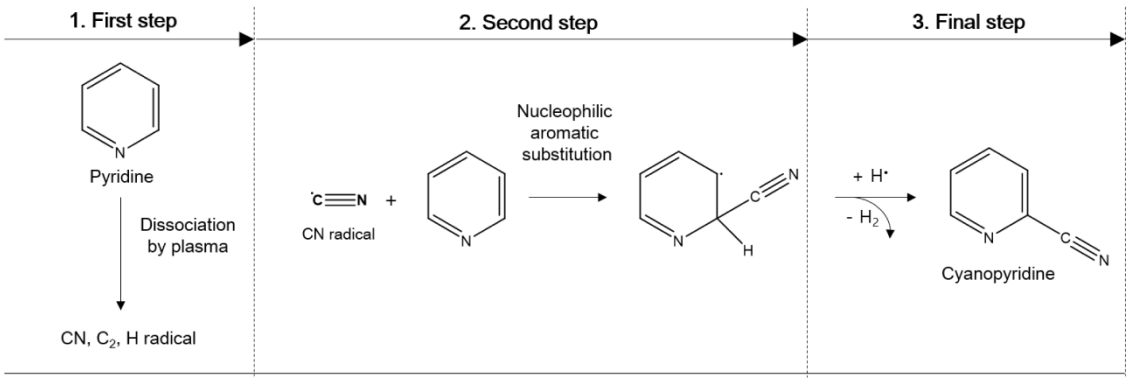

Figure 2.3 Reaction pathway of pyridine to cyanopyridine in SP.

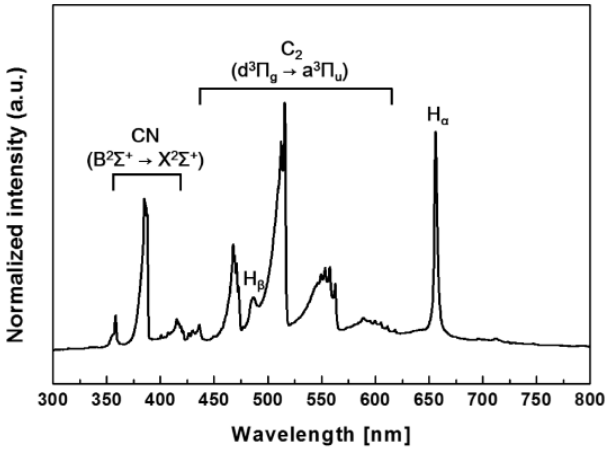

Figure 2.4 OES spectrum of SP in pyridine.

Other reaction pathways of bipyridine, terpyridine and phenanthroline molecule are shown in Fig. 2.5. In this case, the pyridine cation radical might be formed by plasma in the beginning. In the case of the benzene, almost benzene cation radical should be generated from at the interface of plasma/liquid phases by electron excitation without fully dissociation. The radical formation occurs easily when the molecule had π-conjugated bonds [25]. The pyridine molecule has π-conjugated system same as benzene, so that SP might form the pyridine cation radical. In the second step, the pyridine cation radical reacts with the pyridine molecule by CH activation. The pyridine cation radical is electrophile and could react with the π-conjugated bonds of pyridine molecule. As a result, a new radical is formed. In the last step, bipyridine and phenanthroline are formed together with H and C_2 radicals, respectively. Also, when the radical reacts with two pyridine molecules continuously, more large size of new radical is formed. Finally, terpyridine could be formed after the new large radical had reacted with H radical. The initial reaction products identified by GC-MS analysis are considered to be synthesized through these reaction pathways due to SP.

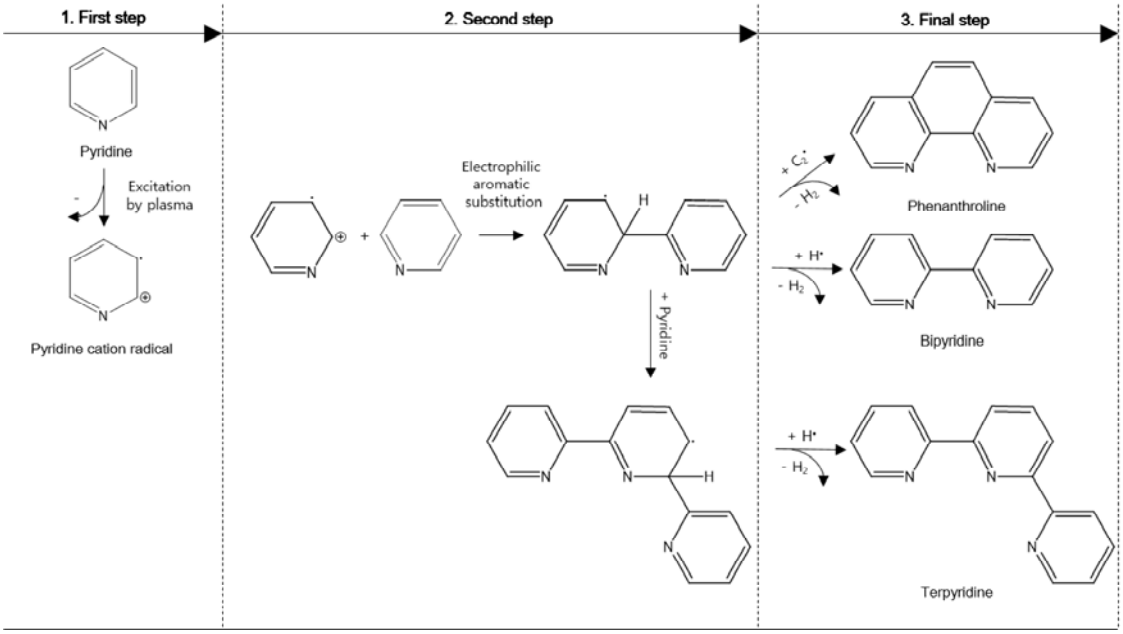

Figure 2.5 Reaction pathway of pyridine to bipyridine, terpyridine, phenanthroline in SP.

Bipyridine and cyanopyridine isomers could be formed depending on the bond position relative to the position of the nitrogen atom. To understand the reason why only some isomers detected by GC-MS were formed, the partial charge of pyridine molecule and the change of the total energy of cyanopyridine and bipyridine isomers were calculated by DFT calculation. In the case of the pyridine molecule, ortho and para position of carbon atom were electropositive (δ^+) as shown in Fig. 2.6 a). The 2- and 4- cyanopyridine molecules were formed because the ortho and para positions could be attacked by the nucleophile as above mentioned. Also, as shown in Fig 2.6 b) 4-cyanopyridine has lower total energy than 2-cyanopyridine as shown in the total energy change diagram from the reactant to cyanopyridine molecules. The result means that the probability of forming 4-cyanopyridine is higher than that of 2-cyanopyridine in the reaction pathway. This result is related to the peak of 4-cyanopyridine observed with high relative intensity in the GC-MS analysis. Fig. 2.6 c) shows

the total energy change of bipyridine isomers after reaction between pyridine molecule and pyridine cation radical. When forming 2,2'-bipyridine molecule, the change of the total energy is -8.768 eV representing the most stable molecular state compared to another bipyridine isomers (2,5-bipyridine: 8.502 eV, 4,4'-bipyridine: 8.550 eV, 2,4-bipyridine: 8.626 eV). Therefore, 2,2'-bipyridine molecule has a high relative intensity peak in the GC-MS.

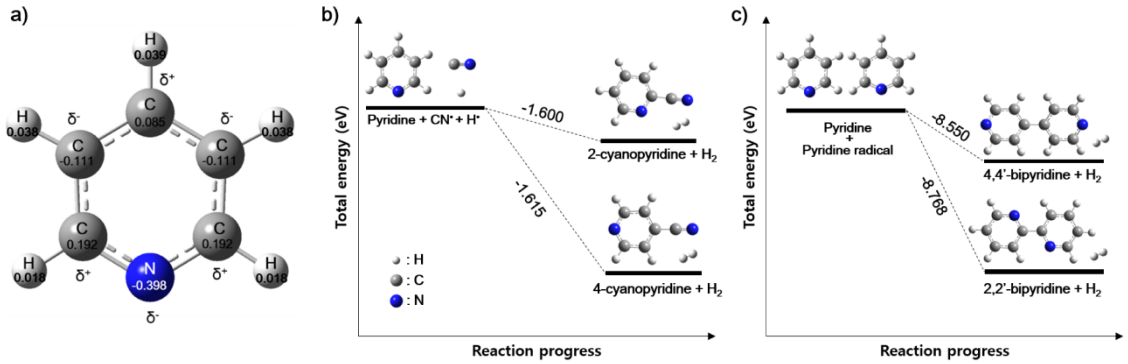

Figure 2.6 a) Partial charge of the optimized geometry for pyridine and total energy diagram of radical reaction for forming isomers of b) cyanopyridine and c) bipyridine by DFT calculation.

Fig 2.7. a) shows the CARS spectra of pyridine before SP and after SP during 1 and 5 sec, respectively, in the range from 1010 to 970 cm^{-1}. In the range, strong band related to pure pyridine was detected at 990 cm^{-1} which associated with the ring breathing mode (ν_1) [26]. The ring breathing mode of occurs owing to a nitrogen atom and two carbon atoms placed in a triangular position in the molecule structure. The intensity of the band rapidly decreases after SP from 30000 to 300 due to the transmittance change of pyridine solution into a brown-dark color, and because the intensity of the CARS signal depends on the laser intensity [27]. After SP, the appearance of a new band around the pyridine band was observed. To understand the

new band, the Raman wavenumber and activity of bipyridine and cyanopyridine molecules were calculated by DFT method. The Raman wavenumber and activity of pyridine, bipyridines, and cyanopyridines are presented in Table. 2.1. As compare with the experimental result, the calculated Raman wavenumber of pyridine was adjusted by a scaling factor determined by the calculation uncertainties [28]. However, the trend of Raman wavenumber value is same for calculation and experiment. The new Raman band with similar signal intensity as the pure pyridine band at 990 cm^{-1} was observed at about 992.5 cm^{-1} after SP during 5 sec. It was considered that this band might be related to 2,2'-bipyridine because the Raman wavenumber was about 3 cm^{-1} higher than that of pyridine and is the most stable molecular state according to the calculation results. Also, despite of the small amount of 2,2' bipyridine, the band intensity could be same as the band of pyridine because the Raman activity is about 4 times stronger than that of pyridine.

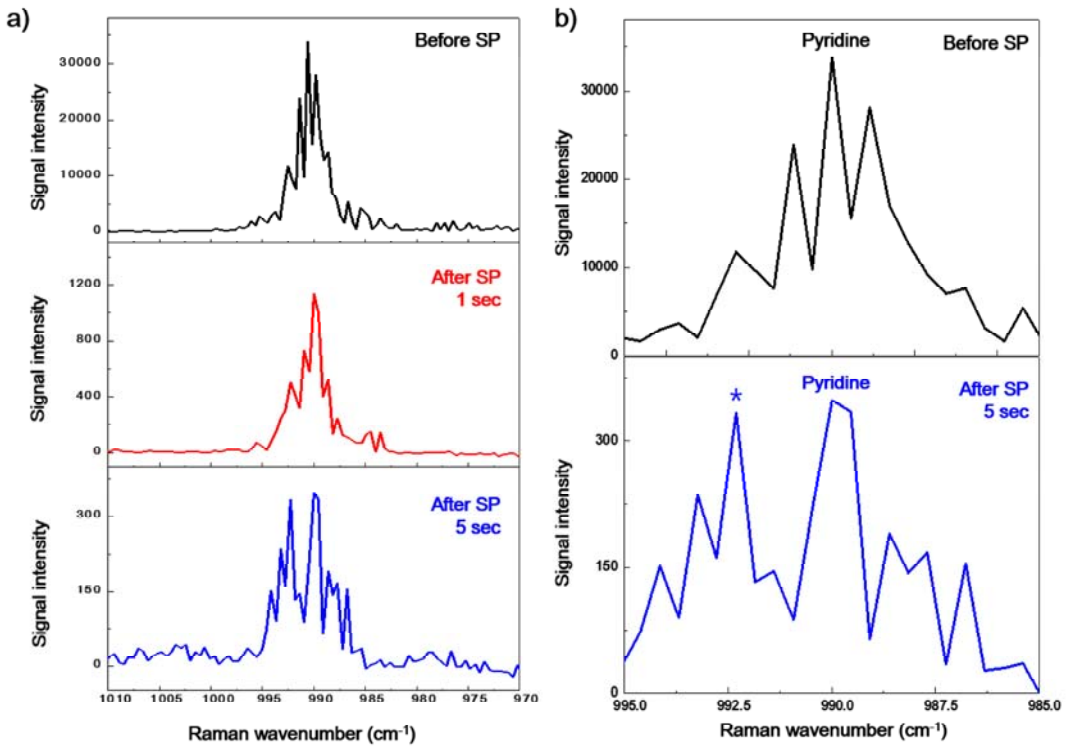

Figure 2.7 a) CARS spectra of the ring breathing mode (ν_1) of pyridine before and after SP in the range from 1010 to 970 cm^{-1}, b) Raman bands between before and after SP during 5 sec in the range from 995 to 985 cm^{-1}.

Table 2.1 Raman wavenumber and activity of cyanopyridine and bipyridine isomers calculated by DFT calculation.

Name of molecule	Raman wavenumber (cm^{-1})	Raman activity
Pyridine	1011.44	30.4930
2-cyanopyridine	1009.12	34.9358
4-cyanopyridine	1009.26	35.5665
2,5- bipyridine	1008.88	92.3737
4,4'- bipyridine	1012.23	62.2108
2,4- bipyridine	1013.93	103.9381
2,2'-bipyridine	1014.35	127.9043

The hetero-carbon materials can be utilized in the field of catalyst and FETs due to their electrical properties. The position and concentration of hetero-atom in the structure are very important because these factors influence to the electrical properties of hetero-carbon nanomaterials [29]. Therefore, it is necessary to understand how to polymerize hetero-organic monomers through SP and how to decide the hetero-atom position by atomic partial charge.

2. 4. Summary

In this study, pyridine was investigated after solution plasma for understanding the initial reactions for the synthesis of hetero-carbon nanomaterial. After few seconds of solution plasma process, cyanopyridine, bipyridine, terpyridine, and phenanthroline molecules were produced from pyridine molecules. In the first step, various kinds of radical species such as CN, C_2, H, and pyridine cation radical were formed in plasma gas phase. In the following step, the CN and the pyridine cation radicals dominantly reacted with the surrounded pyridine molecules by the radical-nucleophilic aromatic substitution and CH activation, respectively. Finally, these reactions produced H and C_2 radicals. It can be concluded that from pyridine large molecules can be formed by radical reaction during solution plasma. Among them, 2,2'-bipyridine was confirmed to have the highest probability of synthesizing by density functional theory calculation. Also, a comparison of the calculated Raman wavenumber of the reaction products and the experimental spectra of coherent anti-Stokes Raman spectroscopy after solution plasma revealed that the new observed band can be associated with 2,2'-bipyridine.

References

1. K.Gong, F.Du, Z.Xia, M.Durstock, L.Dai, Science 323, 760 (2009)
2. D. Guo, R. Shibuya, C. Akiba, S. Saji, T. Kondo, J. Nakamura, Science 351, 361 (2016)
3. H. Wang, T. Maiyalagan, X. Wang, ACS Catal. 2, 781 (2012)
4. H. Wang, Y. Zaho, F. Cheng, Z. Tao, J. Cehn, Catal. Sci. Technol. 6, 3443 (2016)
5. N. Fechler, C. Zussblatt, R. Rothe, R. Schlogl, M. Willinger, B. Chmelka, M. Antonietti, Adv. Mater. 28, 1287 (2016)
6. M. Arjmand, K. Chizari, B. Krause, P. Potschke, U. Sundararaj, Carbon 98, 358 (2016)
7. J. Kang, O. Lun. Li, N. Saito, Carbon 60, 292 (2013)
8. K. Hyun, N. Saito, Sci, Rep. 7, 3825 (2017)
9. G. Panomsuwan, N. Saito, T. Ishizaki, Phys. Chem. Chem. Phys. 17, 6227 (2015)
10. O. Takai, Pure Appl. Chem. 80, 2003 (2008)
11. N. Saito, J. Hieda, O. Takai, Thin Solid Films 518, 912 (2009)
12. D.W. Kim, O.L. Li, N. Saito, Phys. Chem. Chem. Phys. 17, 407 (2015)
13. G. Panomsuwan, S. Chiba, Y. Kaneko, N. Saito, T. Ishizaki, J. Mater. Chem. A. 2, 18677 (2014)
14. G. Panomsuwan, N. Saito, T. Ishizaki, Carbon 98, 411 (2016)
15. F. El-Diasty, Vibrational Spectroscopy 55, 1 (2011)
16. Gaussian 09, Revision D.01, Frisch, M. J. et al. Gaussian, Inc., Wallingford CT, 2009.
17. M.A. Bratescu, J. Hieda, T. Umemura, N. Saito, O. Takai, J. Vac. Sci. Technol. A. 29, 031302 (2011)
18. T. Sudare, T. Ueno, A. Watthanaphanit, N. Saito, J. Phys. Chem. A. 119, 11668 (2015)
19. H.S. Lee, M.A. Bratescu, T. Ueno, N. Saito, RSC Adv. 4, 51758 (2014)
20. A.E. Lefohn, N.M. Mackie, E.R. Fisher, Plasmas and Polymers 3, 197 (1998)
21. E. Aldea, A.P. Caricato, G. Dinescu, A. Luches, A. Perrone, Jpn. J. Appl. Phys. 36, 4686 (1997)
22. S.S. Harilal, R.C. Issac, C.V. Bindhu, V.P.N. Nampoori, C.P.G. Vallabhan, J. Phys. D: Appl. Phys. 30, 1703 (1997)

23. A. Kramida, Y. Ralchenko, J. Reader and NIST ASD Team (2016). NIST Atomic Spectra Database (version 5.4)
24. R.N .Johnson, A.G. Farnham, R.A. Clendinning, W.F. Hale, C.N. Merriam, J. Polym. Sci. A. 5, 2375 (1967)
25. T. Morishita, T. Ueno, G. Panomsuwan, J. Hieda, A. Youshida, M.A. Bratescu, N Saito, Sci. Rep. 6, 36880 (2016)
26. R. Mierzecki, J. Raman Spectrosc. 17, 35 (1986)
27. C.L. Evans, X.S. Xie, Annu. Rev. Anal. Chem 1, 883 (2008)
28. A.P. Scott, L. Radom, J. Phys. Chem. 100, 16502 (1996)
29. W. An, C.H. Turner, J. Phys. Chem. C, 113, 7069 (2009)

Chapter. 3

Quantitative Spectrochemical Analysis of Solution Plasma in Aromatic Molecules

Chapter. 3

Quantitative Spectrochemical Analysis of Solution Plasma in Aromatic Molecules

3. 1. Introduction

A non-thermal discharge in the gas generating from liquid evaporation is called solution plasma (SP). The liquid can be water, water solutions, or several organic solvents [1-3]. In the experiments, types of solutions, materials and geometries of electrodes, reactor configurations, and power supplies decides different characteristics of plasma with the final properties of the synthesized solid material. In previous research, two main types of plasma in aqueous and organic solutions have been studied.

In general, plasma in water has been investigated since 1899 for astronomical purposes related to the interpretation of the emission spectra of stars [4]. In 1952, an exciting experiment, i.e., the action of electrical discharge on a combination of methane, ammonia, water, and hydrogen showed a significant yield of amino, hydroxyl, and aliphatic acids [5]. Recently this experiment was resumed to demonstrate the abiotic synthesis of amino acids and focus on illustrating the origin and evolution of life on Earth [6].

Various type approaches of the SP process in both aqueous and organic solutions have been intensively considered for water purification and sterilization [3,7] polymerization [8], surface modification [9], and nanoparticles synthesis [10-12]. Recently, in our laboratory, a simple and environment friendly SP method was utilized to synthesize nanoparticles and

nanostructures with controlled size, content, and crystallinity [13-16]. The prepared nanocomposite materials with a defined utility such as the absorption of toxic substances or high electrical conductivity [17, 18]. Synthesis of nano carbon and hetero nano carbon materials from hetero-arenes for using catalytic effect as oxygen reduction reaction (ORR) was conducted as a challenge of SP process [19, 20].

SP is composed of the plasma gas phase, the surrounding liquid, the electrodes, and the corresponding interfaces gas/liquid, gas/electrode, and liquid/electrode. In the plasma gas phase, the molecules are excited, ionized, and dissociated. In the organic solutions, polymerization of monomers and formation of polycyclic aromatic hydrocarbon occurred by the reactions of decomposition and recombination [8,19,20]. Also, the permanent exchanges of radicals, ions, and molecules are generated between the plasma gas and liquid phases. Sometimes the synthesized solid material is deposited at the electrodes changing the SP electrical characteristics during the process. The electrode erosion modifies not only plasma during the operation but also the physical and chemical characteristics of the synthesized material [15, 21].

For the effective utilizing solution plasma for material synthesis, a deep understanding of the mechanism on synthesis procedure by solution plasma is necessary and a quantitative diagnostic analysis of both phases (plasma, liquid) could help to understand of the SP process. In the previous studies, electrical measurements to check waveform and optical emission spectroscopy for identifying radicals from the plasma were conducted in the aqueous solution [7,22,23]. For the organic solutions, the liquid and gas chromatography was additionally utilized to confirm the chemical compounds formed after the SP in the liquid phase [6,8,24,25]. However, previous methods as emission spectroscopy and liquid chromatography were

provided only qualitative information. For instance, for water sterilization systems using SP, the hydroxyl radical efficiently killed the bacteria. Therefore, number density of OH radical dependence on water pH and electrical characteristics should be known [7]. That is why the broadband absorption spectroscopy (BAS) method was developed and applied to plasma in aqueous solutions as a quantitative analysis of the OH radical [26].

Recently, a considerable attention have been paid for the effective fabrication of hetero-carbon nanomaterials to apply catalysts or electrodes in batteries [19, 20, 27]. By SP method, carbon material was generated from the plasma in the liquid. Therefore, a quantitative measurement of the number density of molecules and radicals in the plasma is required, analysis of liquid was also needed. Therefore, the atoms, molecules, and radicals from the SP were confirmed using different spectroscopic techniques, as classical optical emission, gas-chromatography mass spectroscopy (GC-MS), BAS in UV-visible spectral region, and electron spin resonance (ESR). The BAS diagnostics method provides a quantitative measurement of the number densities of carbon and cyano radicals on the ground state and hydrogen molecules on an excited state. Furthermore, the chemical composition of the liquid was in-situ measured by absorption spectroscopy. Tens micromoles of arenes and heteroarenes in the liquid phase were confirmed and the chemical reactions for the formation of these compounds were explained. Since the properties of the aromatic molecule is quite important factors in SP process, comparisons among benzene, pyridine, and aniline have been carried out. In SP in benzene, the phenyl radical which is essential in new chemical compounds formation was detected by ESR. The atomic composition of the final carbon solid phase, separately analyzed, was associated with the plasma gas composition. The paper explains the highest production rate of solid carbon material obtained in the case of SP in benzene, which

contains the largest number density of carbon molecules compared to pyridine and aniline. Furthermore, it is shown that the thermodynamic properties of benzene are favorable for obtaining a high molecular carbon density, in contrast with pyridine and aniline.

3.2 Experiment and methods

3.2.1 Experimental procedure

The experimental setup of SP and diagnosis is presented in Fig. 1. The reactor as a quartz beaker with two lateral holes with silicon stoppers were used to fix the metal electrodes. The electrodes are made from 1 mm diameter nickel wire (99.9% purity, Nilaco) covered with insulating ceramic tubes except for a small tip (~1 mm) where the discharge occurs. The distance of the nickel electrodes gap was fixed at 1 ± 0.1 mm. A volume of 30 ml of benzene, pyridine, or aniline (purchased from Kanto Chemicals) was processed by SP during ten minutes. To apply the energy into solution, a bipolar pulsed power supply (MPP-HV04, Kurita) was employed. During the discharge, the voltage was kept about 1.3 kV with 20 kHz of repetition and 1.0 μs of pulse width. A high-voltage probe (P6015A, Tektronix) and a current probe (PR30, LEM) on an oscilloscope (TDS 2014C, Tektronix) were used to record the waveform of voltage and current, respectively.

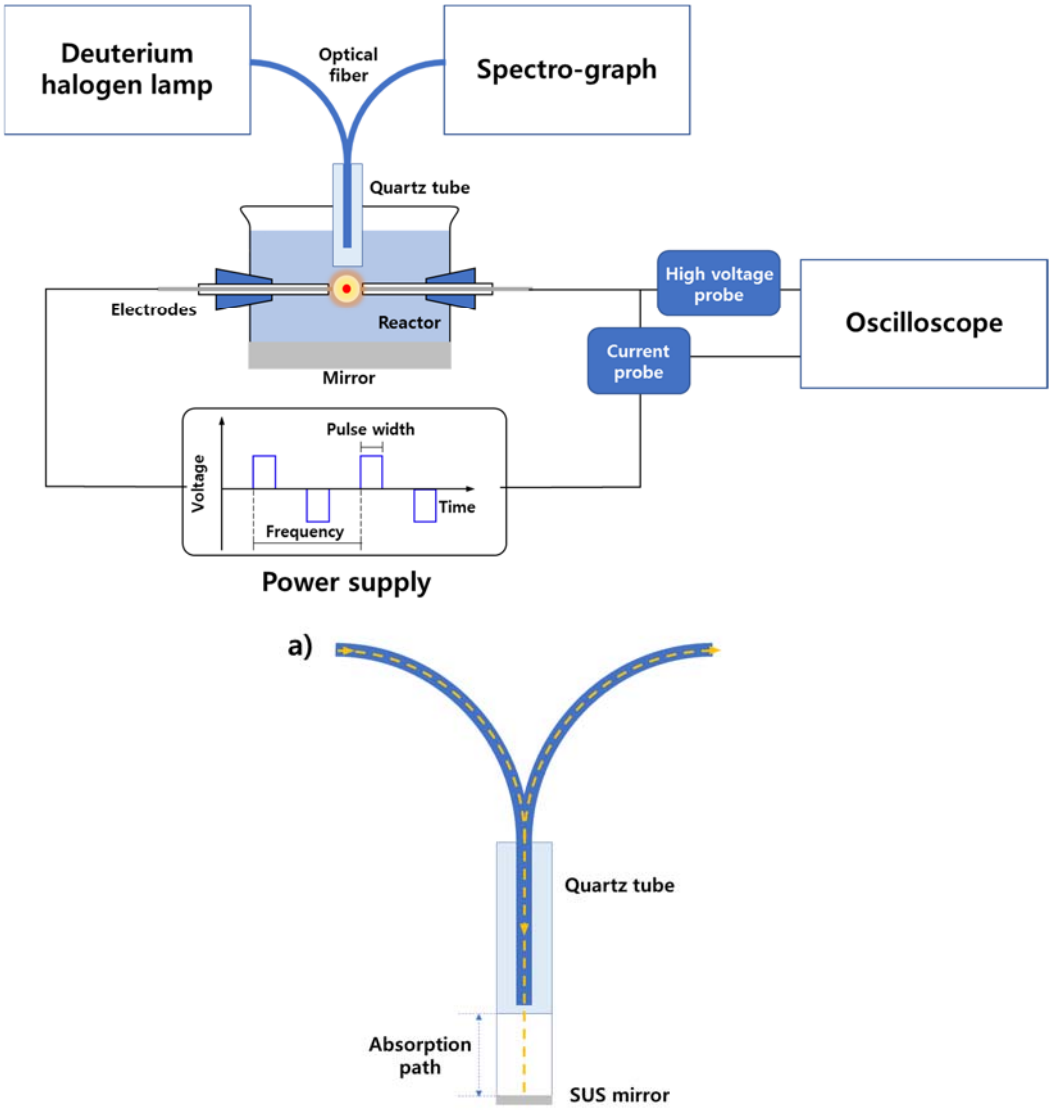

Figure 3.1. The SP experimental set-up and the schematic arrangement of BAS-gas.

Light from the broadband source (Deuterium Halogen Lamp) passes through the solution and plasma gas, reflects in the mirror, and goes back into the fiber to the spectrograph. The voltage and the current probes monitor the SP electrical characteristics. (a) Construction of the optical absorption probe for the BAS-sol method. The quartz tube surrounding the fiber ended with a window coupled with a stainless steel mirror spaced apart at 5 mm from the window. In this space, the solution penetrates and is analyzed.

The BAS method was used in the UV-vis spectral range, to measure the number density of kinds of molecules and radicals in the plasma gas. Also, chemical compounds formed during the SP into the liquid was confirmed. These methods were named BAS-gas and BAS-sol, respectively. A bifurcated optical fiber (Thorlabs, Inc.), optical components (lens and mirrors), a broadband light source (AvaLight DHS, Avantes, Inc.), and a spectrograph (USB Ocean Optics, Inc.) were employed.

In the case of BAS-gas, the light from the broadband source coupled with the bifurcated optical fiber passes through the solution and plasma gas, is reflected on the bottom mirror, and returns into the optical fiber coupled with the spectrograph. The bifurcated optical fiber was introduced into a silica tube with a sealed window to avoid contamination of fiber. In the case of BAS-sol, a particular optical probe was assembled. The fused silica tube surrounding the fiber ended with a window coupled with stainless steel (SUS) mirror spaced apart at 5 mm from the window. In the space between the window and the SUS mirror, the solution is analyzed. For the BAS-sol method, the spectrograph was set in absorption mode measurement. In both experiments, a 5 m length optical fiber which couples SP with the spectrograph was used, to diminish as much as possible the electrical noise from SP and power supply during acquisition.

Ex-situ measurements by GC-MS (JEOL, JMS-Q1050GC) offered the information of the chemical compounds obtained by BAS-sol. The liquid samples were collected from the solution as close as possible to the discharge position. The GC-MS conditions were followed that of our previous measurements [25].

The phenyl radical which is causing chemical reactions in benzene during SP was confirmed by ex-situ ESR spectroscopy (JEOL, JES-FA200). N-tert-Butyl-alpha-

phenylnitrone (PBN) is employed as a spin trap chemical agent to check the radicals used in 10 wt%. During SP, liquid samples were collected, mixed with PBN, and analyzed by ESR. The ESR measuring parameters were as followed, 336 mT of the magnetic field, 10 mT of sweep, 0.35 mT of modulation, 0.1 s of the time constant, and microwave power was controlled up to 10 mW.

The solid carbon materials were prepared after filtration and dried in oven at a temperature over 10°C than the boiling point of the organic solvents. The atomic composition of the solid material obtained after SP was determined by PerkinElmer 2400 II CHNS/O elemental analyzer, at 980°C. The solid carbon material was used for establishing the production rate.

3.2.2 Data evaluation

The optical absorption path length (l) in BAS-gas measurements was estimated to be 0.1±0.05 cm. This value is a very rough approximation due to plasma instabilities, and therefore the discharge size was difficult to be known with high accuracy. In BAS-sol measurements, the path length was set to 1 cm, the distance between the window and SUS mirror multiplied by two. From BAS-sol, the molar concentration (c) of the newly formed chemical compounds from the solution was calculated using the Beer-Lambert law of absorption (A), $c=A/\varepsilon l$, where ε is the molar extinction coefficient known from the database [28]. The reference was the spectrum of the broadband light source passing through the solution, without plasma.

In the case of BAS-gas measurements, the concentration of radicals and molecules from plasma gas was obtained by the integrated absorption over the band knowing the transition oscillator strength as [29]

$$\int absorption\ band\ \frac{I_0 - I(\lambda)}{I_0} d\lambda = 8.85\ X\ 10^{-20} \cdot {\lambda_0}^2 \cdot f_{v'v''} \cdot n \cdot l$$

, where λ_0 is the average wavelength of absorption band in nm, the oscillator strength of the transition is given $f_{v'v''}$, n is number density of species in cm^{-3} (=$c$$N_A$, with N_A is Avogadro number), I_0 and I(λ) are the light intensity before and after passing the sample, respectively. The symbols v' and v'' mean the vibrational quantum numbers. The absorption length l is expressed in cm. The absorbance spectrum was calculated considering subtraction of plasma emission as [29]

$$-\log \frac{I_{S+SP} - I_{SP}}{I_S} = A$$

where I_{S+SP} means SP and broadband source emission, I_{SP} is only SP emission when the shutter of the broadband source is off and Is is the emission from the broadband source. The integration time was set at 100 ms, which corresponds to an average spectrum over 2000 positive pulses. The measurements were repeated at least ten times, a new solution was employed in every time. The excitation temperature (T_{exc}) was calculated from the intensity ratio of the hydrogen emission lines (486.1, 656.3 nm) with the emission intensities after the continuum background radiation subtraction.

In the case of electron density which is a significant parameter of SP calculated using the line broadening of the H_β line (486.1 nm). However, in this experiment, H_α line at 656.4 nm was considered due to the overlap of the molecular emission bands with H_β line. The electron

density (n_e in cm^{-3}) calculation was conducted after the deconvolution of the spectral line considering effects of different broadening using the equation [30, 31]

$$\mathrm{FWHM} = 1.647 \times \left(\frac{n_e}{10}\right)^{0.67965}$$

Full width at half maximum of spectral line is given FWHM, expressed in nm. The total input energy per one pulse was calculated from the integration of the oscilloscope waveforms of the voltage and current over the pulse duration.

3. 3. Results and discussion

3. 3. 1. Electrical breakdown and quantitative spectrochemical analysis of SP gas phase

In this section, the SP electrical breakdown in benzene, pyridine, and aniline and the number density of carbon and cyano radicals and hydrogen molecule in the plasma phase were discussed. The analyzed results for the breakdown voltage at 20 kHz and 1 μs (V_b), total input energy per pulse (W), electron density (n_e), excitation temperature (T_{ext}), and production rate (P) and production efficiency (P_{eff}) were presented.

Table 3.1. Breakdown voltage at 20 kHz and 1 μs (V_b), total input energy per pulse (W), electron density (n_e), excitation temperature (T_{ext}), production rate (P) and production efficiency (P_{eff}).

Parameter	Benzene	Pyridine	Aniline
V_b [V]	5000±100	4000±100	4300±100
W [mJ]	0.77±0.01	0.69±0.01	0.68±0.01
n_e [cm^{-3}]	(8.8±1)x10^{16}	(8.8±1)x10^{16}	(8.8±1)x10^{16}
T_{exc} [eV]	0.65±0.08	0.63±0.08	0.41±0.08
P [mg/min]	14.4±0.1	6.0±0.1	7.7±0.1
P_{eff} [J/mg]	63±1	143±1	111±1

The electrical waveforms (current and voltage) corresponding to the positive pulse in the SP of benzene, pyridine, and aniline are presented in Figure 3.2. In the aspect of scientific and practical reasons, the electrical breakdown in liquid aromatic solvents is still a provocative subject. In a gas discharge, the electron avalanche model inside plasma is well-known on the physical mechanism. When the high voltage applied in the liquid phase, the high density of electrons to be accelerated and dissociation, excitation, and ionization occur except for an applied electric field several orders of magnitude higher than that in atmospheric plasma [3, 32]. Thus, it is required to explain a process of breakdown takes place and how plasma occur in liquids. It could be explained that a phase change by joule heating, i.e., the liquid locally turns into a gas, even in a tiny amount, and then electron avalanches occurred in the gas phase. Thus, thermodynamic and electrical properties of liquid and gas are important points to reveal, furthermore, plasma in solutions can be related to gas discharge physics theory.

The thermodynamic and electrical properties of benzene, pyridine, and aniline are given in Table 3.2 [33]. The boiling point, the specific heat capacity of the liquid and gas at constant pressure and the enthalpy of vaporization show that the energy consumed for gas production from the liquid state has the lowest value for benzene as compared with pyridine and aniline. For example, in order to vaporize for 1 μl solution of benzene, pyridine, and aniline from room temperature, 0.4, 0.6, and 0.8 J are required, respectively. Consequently, the amount of the vaporized benzene is higher than that of pyridine and aniline with assuming that the energy for plasma processes is the same, at the same plasma input energy.

Table 3.2. Thermodynamic and electrical properties of benzene, pyridine, and aniline

Property / Molecule	Benzene	Pyridine	Aniline
Chemical formula	C_6H_6	C_5NH_5	$C_6H_5NH_2$
Ionization energy [eV]	9.24	9.26	7.72
[kcal/mol]	213.1	213.5	178.0
Minimum bond dissociation energy [kcal/mol]	112.9	105.0	80.0
[eV]	4.90	4.55	3.47
Dipole moment [D]	0	2.2	1.53
Dielectric strength [MV/m]	163		17.5
Molecular polarizability [10^{-24} cm^3]	10.24	9.47	11.49
Boiling point [°C]	80.1	115.2	184
Specific heat of liquid at constant pressure [J/mol K]	135.69	193.4	194.0
Specific heat capacity of gas at constant pressure at 300 K [J/mol K]	83.02	157.8	148.7
Enthalpy of vaporization [kJ/mol]	30.72	40.21	51.0
Enthalpy of gas formation [kJ/mol]	82.9	140.2	87.0
Relative permittivity (dielectric constant) of liquid ε_r	2.28	13.26	7.06
Relative permittivity (dielectric constant) of gas ε_{rg}	1.0036	1.0011	1.0012
Thermal conductivity [W/mK]	0.167	0.150	0.172
Density of liquid [g/mL]	0.876	0.9819	1.0217

During one minute SP can provide 924, 828, and 816 J energy in the case of benzene, pyridine, and aniline. In this case, a small amount of the input energy is consumed for vaporization, the rest of the energy being used by processes inside the plasma. The experimental results showed that the total input energy in SP was slightly higher for benzene and approximately equal for pyridine and aniline (Table 3.1).

After breakdown, the current increases, plasma resistance decreases, and voltage decreases. During SP operation the current will be stabilized by the internal impedance of the power supply. The SP generation in aniline and pyridine occurs at a lower breakdown voltage than in benzene. For aniline, the high molecular polarizability and the low ionization potential which determine the facile molecule polarization and electrical breakdown are 11.49×10^{-24} cm^3 and 7.72 eV, respectively. The molecular polarizabilities of benzene and pyridine of 10.24×10^{-24} cm^3 and 9.47×10^{-24} cm^3, respectively, and the ionization energy at 9.24 and 9.26 eV, respectively, indicate that the difference in the breakdown voltage between benzene and pyridine is due to the discrepancy in the dipole moment.

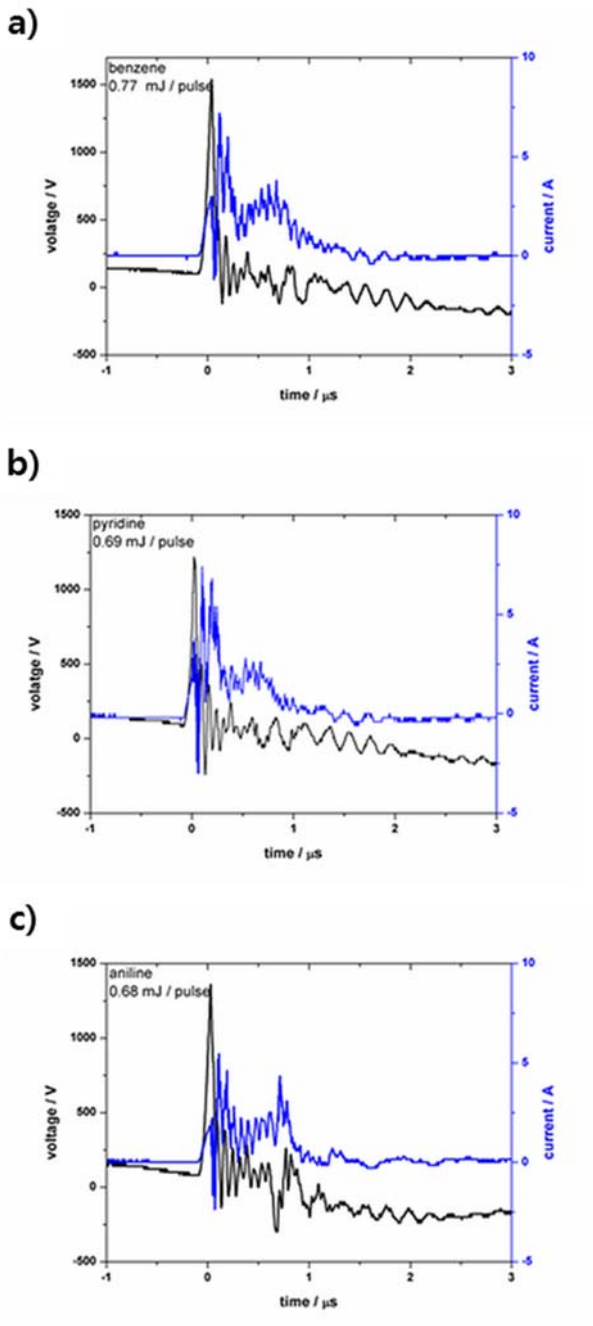

Figure 3.2. Voltage and current waveforms of the positive pulse during discharge in (a) benzene, (b) pyridine, and (c) aniline.

In this section, the quantitative spectroscopic analysis results of gas plasma will be discussed. The results of emission and absorption spectra from SP are presented at Figure 3.3, and the identification of the atoms, molecules, and radicals in the plasma is shown in Table 3.3. The number density of the CN and C_2 radicals in the ground state and H_2 molecules in an excited electronic state in the plasma gas phase was obtained from the absorption spectra. The number density of CN and C_2 radicals and H_2 molecule with the transition oscillator strength are given in Table 3.4. The errors of the number density measurements are large values due to the high instabilities of plasma which decide the evaluation of the absorption path length within 50 % accuracy.

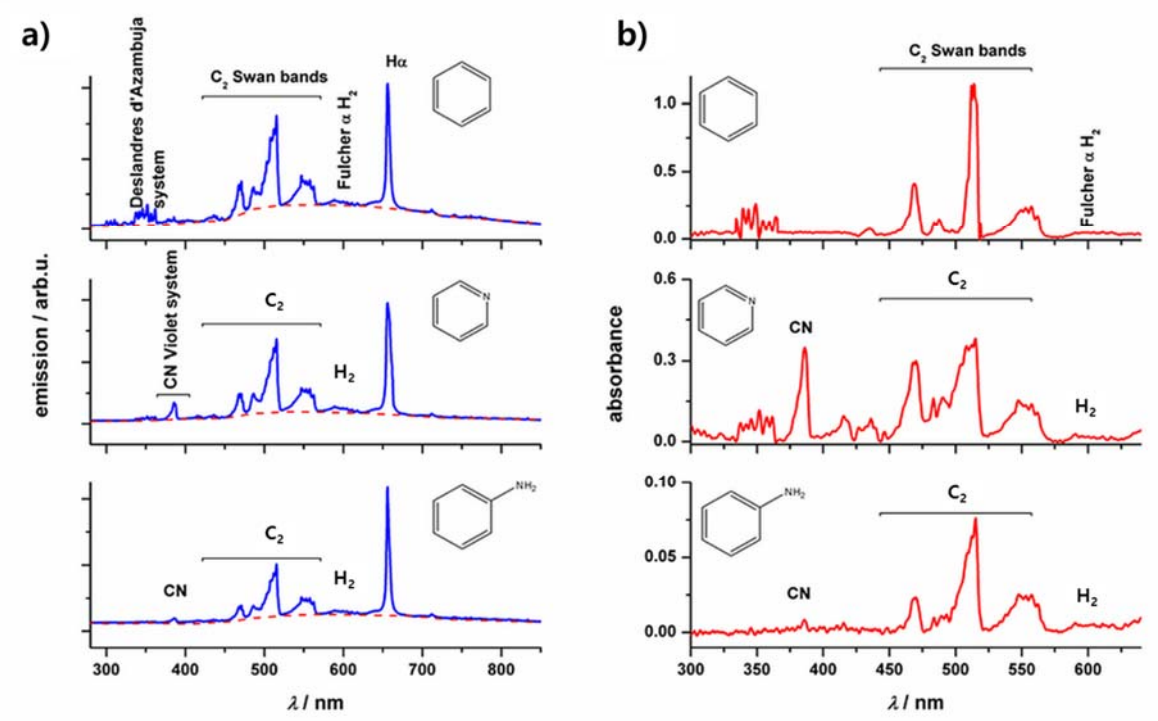

Figure 3.3. (a) Emission and (b) absorption spectra obtained by BAS-gas. In the emission spectra, the dotted red line represents the background radiation. From the absorbance spectra, the number density of C_2 and CN radicals on the ground state, and H_2 molecule on the electronically excited state was determined.

Table 3.3. Transitions of atoms, molecules, and radicals in the emission spectra.

Transition band	Wavelength in nm v'-v"	Transition (upper level – lower level)	Atom, Molecule or Radical	SP
Swan system	516.5 0-0 471.5 2-1 547.0 4-5 558.0 1-2	$d^3\Pi_g - a^3\Pi_u$	C_2	Benzene Pyridine Aniline
Swan system under high pressure	589.9 6-8	$d^3\Pi_g - a^3\Pi_u$	C_2	Benzene Pyridine Aniline
Deslandres d'Azambuja system	385.2 0-0 360.7 1-0 358.7 3-2	$c^1\Pi_g - b^1\Pi_u$	C_2	Benzene Pyridine Aniline
C_3 molecule	405.0	$1\Pi_u - 1\Sigma_g^+$	C_3	Benzene
Violet system	388.3 0-0 415.2 5-6	$B^2\Sigma^+ - X^2\Sigma^+$	CN	Pyridine Aniline
Phenyl radical	504.8		C_6H_5	Benzene
Schuler's T spectrum Diacetylene ion	506.7		$C_4H_2^+$	Benzene
Benzyl radical system	447.0		C_7H_7	Benzene
Benzene cation	545.3 0-0		$C_6H_6^+$	Benzene
Carbon molecule anion	541.6	$^2\Sigma - {}^2\Sigma$	C_2^-	Benzene Pyridine Aniline
Fulcher Hydrogen molecule	600 -630	$d^3\Pi_u^- - a^3\Sigma_g^+$	H_2	Benzene Pyridine Aniline
Balmer series	434.0 486.1 656.3	n = 5-2 n = 4-2 n = 3-2	H H H	Benzene Pyridine Aniline
Carbon	711.5 833.5	$5^3P_0^o - 3^3D_1$ $3^1S_0 - 3^1P_1^o$	C	Benzene Pyridine Aniline

Table 3.4. Number density (in cm^{-3}) of C_2 and CN radicals and H_2 molecules in the plasma gas phase measured by BAS-gas.

Radical	Oscillator strength	Benzene	Pyridine	Aniline
C·≡C· on the ground state $a^3\Pi_u$	0.027	$(2.2\pm1.3)\times10^{16}$	$(6.8\pm4.1)\times10^{15}$	$(1.5\pm0.9)\times10^{15}$
C·≡N on the ground state $X^2\Sigma^+$	0.027	-	$(1.1\pm0.7)\times10^{16}$	$(3.4\pm2.0)\times10^{14}$
H_2 on the excited state $a^3\Sigma_g^+$	0.14	$(1.6\pm1.0)\times10^{14}$	$(5.4\pm3.2)\times10^{13}$	$(1.6\pm1.0)\times10^{13}$

Therefore, the large amount of the evaporated benzene determines the high number density of C_2 in the plasma phase compared to that of pyridine and aniline. Moreover, the slightly higher excitation temperature in SP in benzene cause the smaller fragment formation by a dissociation and an increasing number density of radicals and molecules, consequently. The relative amount of C_2 to benzene, pyridine, and aniline molecules was estimated to be 8×10^{-4}, 3×10^{-4}, and 6×10^{-5}, respectively, as considering Loschmidt constant.

During the SP process in pyridine and aniline, the CN radical number density was detected to be 1.1×10^{16} and 3.4×10^{14} cm^{-3}, respectively (Table 3.4). The high enthalpy of vaporization and elevated boiling temperature of aniline lead to higher energy to vaporize and then operate the SP as compared with pyridine. At last, in the SP in aniline, it is confirmed that the number density of CN and C_2 radicals in plasma gas is lower than pyridine.

In all the UV-vis emission spectra, a broadband background radiation was observed due to clusters and nanoparticles of carbon material [45]. The absence of the emissions from CH,

NH radicals, and N_2 molecule in the plasma gas of pyridine and aniline informs that the dissociation of molecules occurs by breaking the bond between carbon and hydrogen or nitrogen. The hydrogen molecule observed in the spectra and its density and an excited state from ground state are 2 to 16×10^{13} cm^{-3} and 12 eV, repectively, confirming the hydrogen dissociation from the molecules [43]. In the case of benzene, the bond dissociation energy of the first hydrogen is 4.9 eV and second dissociation energy is ranging from 3.38 to 4.72 eV relying on the hydrogen position. Therefore, phenyl radical can be produced easily in the plasma gas phase in benzene and it was observed in the emission spectrum. The minimum dissociation bond energy of a hydrogen atom of pyridine is 4.55 eV and aniline needs only 3.47 eV to separate a hydrogen atom from the amino group [46-48]. In the case of a non-thermal plasma as SP, the tail of the electron energy probability function incorporates electrons with energies of about 10 eV, which can lead the ionization and dissociation of these aromatic molecules [49]. Furthermore, the electron density was found to be the same, within the limits of experimental errors, using the evaluation from the hydrogen line broadening in all plasmas. Thus, the increasement on number density of C_2 and CN radicals from plasma in benzene and pyridine can be strongly explained by the profitable thermodynamic parameters of these aromatic molecules compared to aniline. In addition, the nickel emission lines were not detected in all the UV-vis spectra, indicating that electrode sputtering is insignificant in the SP process.

3. 3. 2. In-situ quantitative spectrochemical analysis of SP liquid phase

The reactions for the formation of low molecular weight chemical compounds in the solution *in-situ* BAS-sol results, and ESR detection result of the phenyl radical are explained.

In-situ BAS-sol results shows the molar concentration of the newly formed compounds into the solution in different times. The transmission of the solution rapidly decreased, making impossible the absorbance measurement in range around 200 to 800 nm due to the solid carbon material obtained after 10 minutes of SP process. Figure 3.4 presents in-situ BAS-sol results of the quantitative analysis in (a) benzene, (b) pyridine, and (c) aniline. The maximum molar concentration of molecules was obtained from the absorbance considering ε [28].

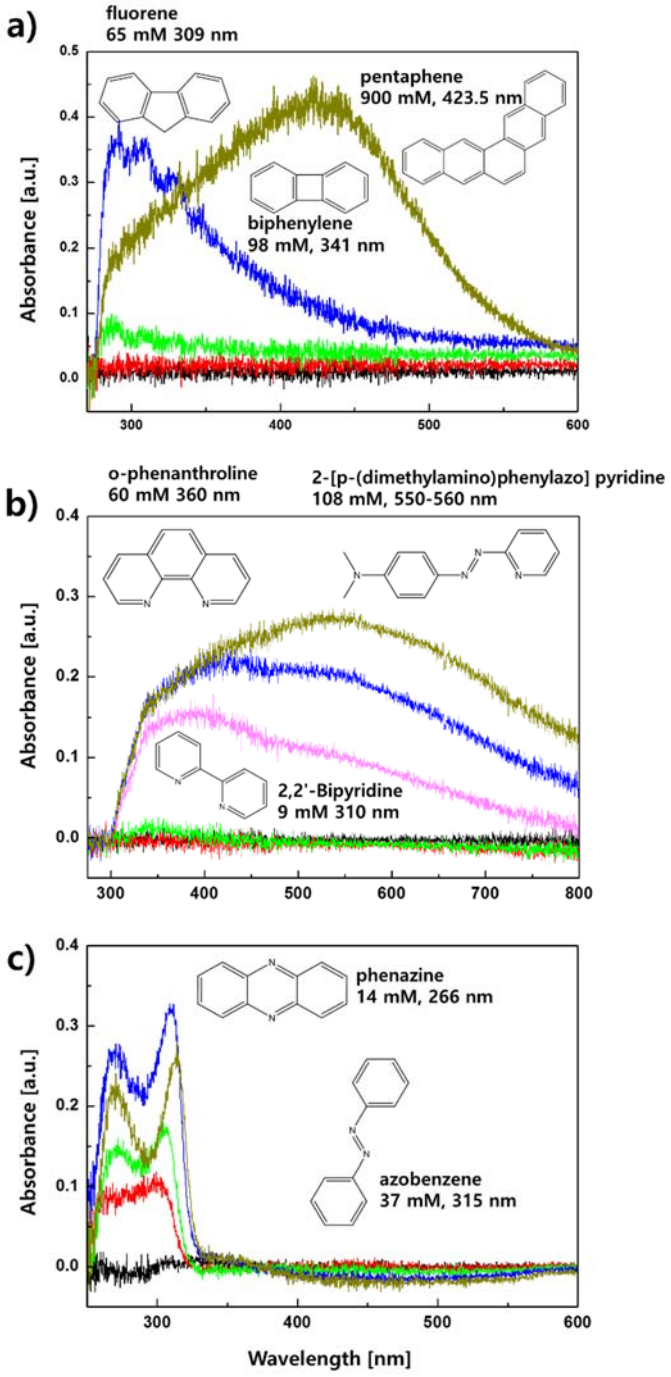

Figure 3.4. In-situ BAS-sol results in (a) benzene, (b) pyridine, and (c) aniline.

New low molecular weight chemical compounds were detected in the solution during SP process and the molar concentration was determined using the absorbance value.

The molar concentration of newly formed molecules in the solution is in the range of from 9 to 900 μM. The results of GC-MS analysis confirmed the small weight molecules obtained by in-situ BAS-sol. In the case of benzene and pyridine, the BAS-sol results of absorbance were matched with our previous GC-MS measurements [25, 50].

The reaction of the phenyl radical formed by SP with benzene conducts to a formation of biphenyl, which has been confirmed by GC-MS result. Biphenylene and fluorene could be formed from biphenyl or directly from benzene molecule and phenyl radical [51]. In SP in benzene, the presence of the phenyl radical was confirmed by emission spectroscopy in plasma gas phase and ESR measurement of liquid phases, respectively. Figure 3.5 presents that the reaction of PBN and a phenyl radical is shown together with the ESR signal of the resulted radical [52]. The list of reactions for the formation of small weight molecules in solutions are given in Table 3.5. The chemical reactions show that carbon atom and molecule radicals contribute to the formation of fluorine and o-phenanthroline, demonstrating the role of gas plasma in chemical synthesis.

Table 3.5. The reactions for the formation of small weight molecules into the solution derived from in-situ BAS-sol results (Figure 3.4).

Chemical formula	Reaction	Molar concentration [μM]
Fluorene $C_{13}H_{10}$	$C_6H_6+C_6H_5\cdot+C\cdot \xrightarrow{H\cdot} C_{13}H_{10}$	65±4
Biphenylene $C_{12}H_8$	$C_6H_6+C_6H_5\cdot \xrightarrow{3H\cdot} C_{12}H_8$	98±3
2,2'-Bipyridine $C_{10}H_8N_2$	$C_5H_5N+C_5H_5N \xrightarrow{2H\cdot} C_{10}H_8N_2$	9.0±0.7
o-phenanthroline $C_{12}H_8N_2$	$C_5H_5N+C_5H_5N+C_2\cdot \xrightarrow{2H\cdot} C_{12}H_8N_2$	60±6
Phenazine $C_{12}H_8N_2$	$C_6H_5NH_2+C_6H_5NH_2 \xrightarrow{3H_2} C_{12}H_8N_2$	14±3
Azobenzene $C_{12}H_{10}N_2$	$C_6H_5NH_2+C_6H_5NH_2 \xrightarrow{2H_2} C_{12}H_{10}N_2$	37±3

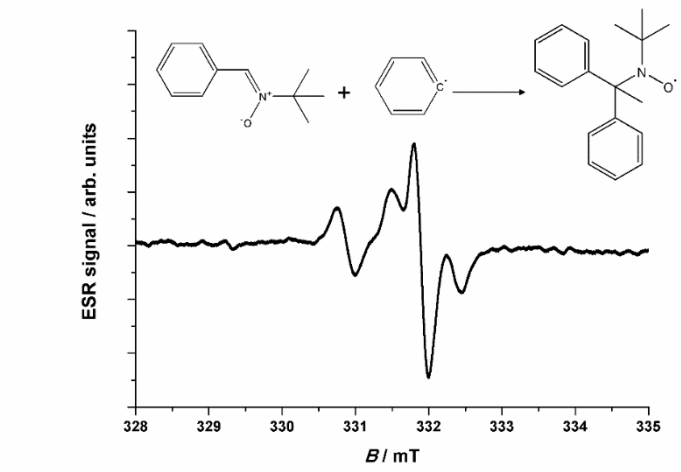

Figure 3.5. The ESR signal of the PBN-phenyl radical. The reaction of PBN with phenyl radical is included.

3. 3. 3. The atomic composition of the solid phase

The production rate of solid carbon material from solution plasma in benzene is twice faster as compared with pyridine and aniline. The density of C_2 in the plasma gas can determine the production rate (Table 3.1). The large production rate of solid carbon material from benzene by SP as compared with other hydrocarbons was also reported [25]. The atomic composition of the solid carbon material prepared from benzene, pyridine, and aniline in SP is given in Figure 3.6. The “H/C before and N/C before” refer to the atomic composition ratio of the liquid aromatic compounds, before plasma processing.

The results of atomic composition shows that hydrogen ratio in the carbon material rapidly decreased; the decrease of nitrogen is almost half as compared to that of hydrogen for pyridine and aniline. The high concentration of remained hydrogen in the solid carbon material generally means that the carbon structure is an amorphous structure with low electrical conductivity due to a preponderant sp3 carbon structure [20, 25]. The graphene-like sheet structure also synthesized by using SP in aromatic molecules, but amount were quite small [27].

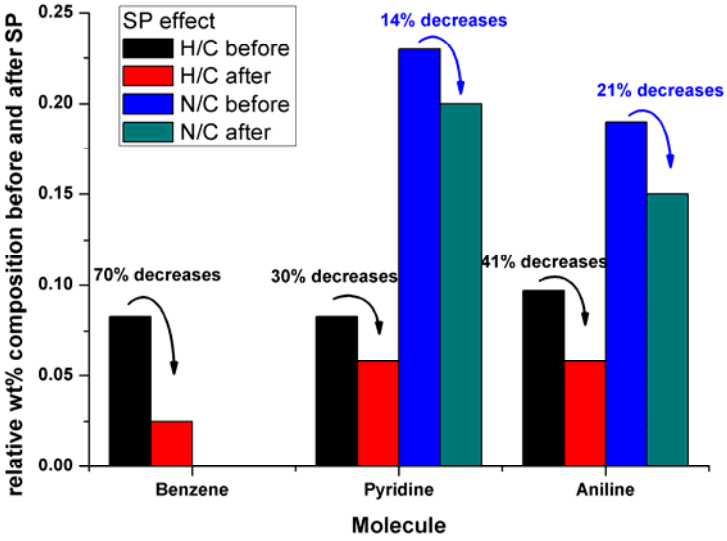

Figure 3.6. Atomic composition analysis of the solid carbon material synthesized from benzene, pyridine, and aniline in SP.

3.4 Summary

The presented analysis methods are simple and provide physical and chemical information on the plasma gas and solution phases. The SP electrical breakdown and operation considering the thermodynamic and electrical characteristics of the aromatic molecules were explained. A quantitative analysis of the radicals and molecules has been performed in the plasma during the discharge and after discharge. The newly formed chemical compounds by SP were confirmed by GC-MS method and their concentration were tens micromoles. The phenyl radical is one of the main initiators for forming a new molecules during SP in benzene and it was confirmed by ESR measurement.

The SP showed the potential for nanocarbon synthesis method as graphene and nitrogen-doped-graphene starting from arenes and heteroarenes. However, considerable attention should be still needed to mend the crystallinity and electrical conductivity of nano carbon through a better hydrogen release during the SP process. Therefore, diagnostics of SP process are required and the quantitative measurements of the radicals and the chemical compounds generated into the solution might facilitate the strategy to material design for prefer purposes [8,19,20,25,27].

References

1. N. Saito, M. A. Bratescu, K. Hashimi, Jap. J. Appl. Phys. 57, 0102A4 (2018)

2. O. Takai, Pure Appl. Chem. 80, 2003 (2008)

3. P. Vanraes, A. Bogaerts, Appl. Phys. Rev. 53, 031103 (2018)

4. J. Wilsing, Astrophysical Journal 10, 113 (1899)

5. S. L. Miller, Science 117, 528 (1953)

6. L. Jiang, P. Dziedzic, Z. Spacil, G. Zhao, L. Nilsson, L. L. Ilag, A. Cordova, Scientific Reports 4, 6769 (2014)

7. B. R. Locke, M. Sato, P. Sunka, M. R. Hoffmann, J. S. Chang, Ind. Eng. Chem. Res. 45, 882 (2006)

8. J. Senthilnathan, C. Weng, J. Liao, M. Yoshimura, Scientific Reports 3, 2414 (2013)

9. R. Joshi, R. D. Schulze, A. Meyer-Plath, J. F. Friedrich, Plasma Processes and Polym. 5, 695 (2008)

10. Z. Abdullaeva, E. Omurzak, C. Iwamoto, H. Okudera, M. Koinuma, S. Takebe, S. Sulaimankulovaf, T. Mashimo, RSC Adv. 3, 513 (2013)

11. S. H. Kim, H. S. Choi, K. D. Jung, Cryst. Growth Des. 16, 1387 (2016)

12. G. Saito, S. Hosokai, M. Tsubota, T. Akiyama, Cryst. Growth Des. 12, 2455 (2012)

13. J. Hieda, N. Saito, O. Takai, J. Vac. Sci. Technol. 26, 854 (2008)

14. M. A. Bratescu, S. P. Cho, N. Saito, O. Takai, J. Phys. Chem. C 115, 24569 (2011)

15. M. A. Bratescu, N. Saito, O. Takai, J. Alloys Compd. 562, 74 (2013)

16. M. A. Bratescu, N. Saito, J. Phys. Chem. C 117, 26804 (2013)

17. S. Chae, M. A. Bratescu, N. Saito, J. Phys. Chem. C 121, 23793 (2017)

18. H. Kim, A. Watthanaphanit, N. Saito, ACS Sustainable Chem. Eng. 5, 5842 (2017)

19. S. Lee, Y. Heo, M. A. Bratescu, T. Ueno, N. Saito, Phys. Chem. Chem. Phys. 19, 15264 (2017)

20. T. Ishizaki, S. Chiba, Y. Kaneko, G. Panomsuwan, J. Mater. Chem. A 2, 10589 (2014)

21. H. Lee, M. A. Bratescu, T. Ueno, N. Saito, RSC Adv. 4, 51758 (2014)

22. P. Bruggeman, C. Leys, J. Phys. D: Appl. Phys. 42, 053001 (2009)

23. H. M. Jones, E. E. Kunhardt, J. Appl. Phys. 78, 3308 (1995)

24. M. A. Bratescu, J. Hieda, T. Umemura, N. Saito, O. Takai, J. Vac. Sci. Tech. 29, 031302 (2011)

25. T. Morishita, T. Ueno, G. Panomsuwan, J. Hieda, A. Yoshida, M. A. Bratescu, N. Saito, Scientific Reports 6, 36880 (2016)

26. C. Miron, M. A. Bratescu, N. Saito, O, Takai, J. Appl. Phys. 109, 123301 (2011)

27. K. Hyun, N. Saito, Scientific Reports 7, 3825 (2017)

28. K. Hirayama, Handbook of Ultraviolet and Visible Absorption Spectra of Organic Compounds, Fuji Photo Film Research Laboratories, Odawara, Japan, Plenum Press Data Division, New York, (1967)

29. A. N. Goyette, J. E. Lawler, L. W. Anderson, D. M. Gruen, T. G. McCauley, D. Zhou, A. R. Krauss, J. Phys. D Appl. Phys. 31, 1975 (1998)

30. P. Bruggeman, T. Verreycken, M. A. Gonzalez, J. L. Walsh, M. G. Kong, C. Leys, D. C. Schram, J. Phys. D: Appl. Phys. 43, 124005 (2010)

31. M. A. Gigosos, M. A. Gonzalez, V. Cardenoso, Spectrochimica Acta Part B 2003, 58, 1489 (2003)

32. V. I. Ushakov, V. F. Klimkin, S. M. Korobeynikov, Impulse Breakdown of Liquids Power Systems, Chap. 1, Springer Berlin (2007)

33. NIST Chemistry WebBook https://webbook.nist.gov/chemistry/

34. D. L. Kokkin, C. B. Bacskay, T. W. Schmidt, J. Chem. Phys. 126, 084302 (2007)

35. J. E. Mentall, R. W. Nicholls, Proc. Phys. Soc. 86, 873 (1965)

36. R. W. B. Pearse, A. G. Gaydon, Identification of Molecular Spectra, Fourth Edition, Chapman and Hall (1975)

37. M. Ferus, P. Kubelík, A. Knížek, A. Pastorek, J. Sutherland, S. Civiš, Scientific Reports 7, 6275 (2017)

38. R. G. Bennett, F. W. Dalby, J. Chem. Phys. 36, 399 (1962)

39. H. F. Schaefer, T. G. Heil, J. Chem. Phys. 54, 2573 (1971)

40. J. G. Radziszewski, Chem. Phys. Lett. 301, 565 (1999)

41. K. Walter, R. Weinkauft, U. Boesl, E. W. Schlag, Chem. Phys. Lett. 155, 8 (1989)

42. W. S. Cathro, J. C. Mackie, J. Chem. Soc. Faraday 2 69, 237 (1973)

43. D. R. Farley, D. P. Stotler, D. P. Lundberg, S. A. Cohen J. Quant. Spec. & Rad. Transfer 112, 800 (2011)

44. NIST Atomic Lines Spectral Database https://www.nist.gov/pml/atomic-spectra-database.

45. Y. Suda, K. Utaka, M. A. Bratescu, Y. Sakai, J. Tsujino, K. Suzuki, Appl. Phys. A 79, 1331 (2004)

46. G.E. Davico, V. M. Bierbaum, C. H. DePuy, G. B. Ellison, R. R. Squires, J. Am. Chem. Soc. 117, 2590 (1995)

47. C. Barckholtz, T. A. Barckholtz, C. M. Hadad, J. Am. Chem. Soc. 1999, 121, 491.

48. J. A. Kerr, Chemical Rev. 66, 465 (1966)

49. F. Taccogna, G. Dilecce, Eur. Phys. J. D 70, 251 (2016).

50. K. Kim, K. Hashimi, M. A. Bratescu, N. Saito, Nanoscience and Nanotechnology Lett. 10, 814 (2018)

51. B. Shukla, K. Tsuchiya, M. Koshi, J. Phys. Chem. A 115, 5284 (2011)

52. G. R. Buettner, Free Radical Biology&Medicine 3, 259 (1987)

Chapter. 4

Rapid Synthesis of Highly N-doped Carbon Dots through Solution Plasma and their Molecular Detection Properties

Chapter. 4

Rapid Synthesis of Highly N-doped Carbon Dots through Solution Plasma and their Molecular Detection Properties

4. 1. Introduction

The fluorescence-based detectors have become much popular owing to their high sensitivity, portability, and easy operation as compared with the other methods such as gas chromatography [1], surface-enhanced Raman spectroscopy [2], and surface plasmon resonance [3]. Among the various kinds of toxic molecules, the trinitrophenol (TNP), a representative powerful explosive molecule, is worth to be detected. Because the TNP is a toxic substance that can cause irritation of skin and eye, also make a damage to liver and kidney. Although, it is still popularly used in chemical, agricultural, and medical fields [4,5]. More seriously, the significant pollution of soil and aquatic system occur due to high water solubility [6]. Therefore, it is worth to develop an ultra-sensitive TNP detector.

Recently, carbon dots (CDs) in the range of a few nanometers of carbon particles are emerging as a new research field for carbon nanomaterials due to their fluorescence property by quantum confinement effect [7-9]. Thus, the CDs have potential in the fluorescence-based detectors applications. Moreover, their excellent biocompatibility makes them strongly benefit in applying to most application fields without a concerning of toxicity [10,11]. However, the low quantum yield (about 10%) attributed to energy conversion efficiency and an absence of functional groups of pristine carbon dots are critical problems to be solved. Nowadays, the studies of carbon dots have been focused on using the heteroatoms such as nitrogen, sulfur,

and phosphors to enhance their performance [12-14]. The addition of heteroatoms in carbon dots causes specific changes in the electron energy level due to their lone pair of electrons and can be expected additional effects by the functional groups. In order to synthesis, new synthesis methods should be considered. Because hydrothermal and pyrolysis methods, which are represented as a conventional method, take a too long time for synthesis and modification. The solution plasma is an alternative method to solve these problems. During the SP, plenty of reactive species such as a radical, electron, and ion are generated from organic and inorganic substance and it leads to rapid reaction for synthesis material [15]. Through the SP, the pyridine monomers converted to the pyridine oligomer, and the functionalization of nitrile group occurred in only a few seconds [16]. The previous study provides a clue to solve the reason of rapid synthesis rate of the nitrogen-doped carbon dots (NCDs) with rich functional groups. In this study, the NCDs with high N concentration and abundant amino-functional groups were designed to detect the TNP effectively. The increasing of amino-functional groups was expected to enhance the fluorescence detecting performance based on photo-induced electron transfer (PET). Because, the amino-functional group is one of the strongest electron donor groups among the functional groups, so the amino-functional groups could help to transfer of excited electrons in the NCDs. The NCDs synthesized from the pyridine and water mixture for 10 min by SP. The synthesized NCDs were evaluated as a molecular detector for the TNP by fluorescence quenching efficiency, and the effect of the amino-functional group on the sensitivity of the NCDs was confirmed. To reveal the selectivity for the TNP, the quenching efficiencies of NCDs were measured with the other nitro group molecules.

4.2. Experimental procedure

4.2.1 Materials

Pyridine, distilled water, 2,4,6-trinitrophenol (TNP), nitro-benzene (NB), nitronaphtalene (NN), nitroanthracene (NA), nitrofluorene (NF) were purchased from Kanto chemicals.

4.2.2 Synthesis of NCDs

The pyridine (70 mL) with water (30 mL) solution was used to synthesize the NCDs. The mixtures were mixed by a magnetic stirrer for 30 min. After that, the solution plasma was generated in each solution for 10 min. A bipolar pulse power supply (Kurita) used to discharge between the tungsten electrodes (Nilaco) which is covered by ceramic tubes to protect of loss of current. The gap distance between the metal electrodes in the SP reactor was fixed at 0.5 mm. During the discharge, the voltage and current were 2 kV and 1A, respectively and the pulse width and pulse repetition frequency were controlled at 1.0 μs and 50 kHz.

4.2.3 Characteristics

To reveal the size and distribution of NCDS, transmission electron microscopy (TEM, JEM-2500SE, JEOL) was employed. In the case of information on the composition of NCDs, the elemental analysis (CHNS/O2400-2, PerkinElmer) was performed to obtain ratio of C, H, O, N. The X-ray diffractometer (XRD, SmartLab, Rigaku) and Raman spectroscopy (Invia Raman microscope, Renishaw) are used for confirm the diffraction patterns and molecular vibration information. The absorption of NCDs in water was performed using UV-Vis spectrophotometer (UV-3600, Shimadzu). The functional groups on the surface of NCDS were confirmed by Fourier transform infrared spectroscopy (FT-IR, Nicolet 8700, Thermo Fisher). The fluorescence spectra of NCDs were measured using a spectrofluorometer (FP-6600, JASCO).

4.2.4 Quantum yield

The quantum yield of CDs which is related to energy efficiency was obtained by the following equation

$$Q_a = Q_{st} \frac{I_a}{I_{st}} \frac{A_{st}}{A_a} \left(\frac{\eta_a}{\eta_{st}} \right)^2$$

Where the *st* means to a standard molecule of quantum yield, in this study, Rhodamine B, Q_{st} is the quantum yield of Rhodamine B (0.31). In the case of refractive index, since using water both, the value of η_a and η_{st} are same as 1.333 in this study. I_a and I_{st} mean the fluorescence peak integrated area of the NCDs and Rhodamin B, respectively, A and A_{st} represent the corresponding absorbance value of the NCDs and Rhodamin B.

4.2.5 Procedure for detection of nitro group molecules

Various concentrations of the TNP (0, 1, 5, 10, 50, 100, and 500 μM) were added into the NCDs solution to confirm the sensitivity. The experiment for selectivity was performed with the 100 μM of NB, NN, NA, and NF in the NCDs solution. The change of fluorescence of NCDs solutions was revealed with 340 mm of excitation wavelength at room temperature. The quenching constant value (K_{sv}) as the slope (S) of the calibration plot calculated from the Stern-Volmer plots. The limit of detection (LOD, 3σ/S) was obtained where σ is the standard deviation of the blank signal.

4.3. Result & discussion

The shape and size of the NCDs were observed by TEM as shown in figure 4.1(a). The NCDs show the monodispersed spherical shape with 6 nm of average size (the corresponding particle size distribution is shown at fig.4.1(b)). Furthermore, the HRTEM image clearly presented 0.23 nm of lattice spacing of the NCDs. The atomic composition of the NCDs was measured by the atomic analyzer and presented at the table. 4.1. The NCDs synthesized through solution plasma were consisted of carbon, hydrogen, nitrogen, and oxygen. The oxygen composition is due to the water in the precursor solution. When the plasma discharge in water, reactive species was generated such as OH, O radicals detected at 309 and 777 nm, respectively [17]. The radicals lead to a presence of oxygen composition during the synthesis of the NCDs by the SP.

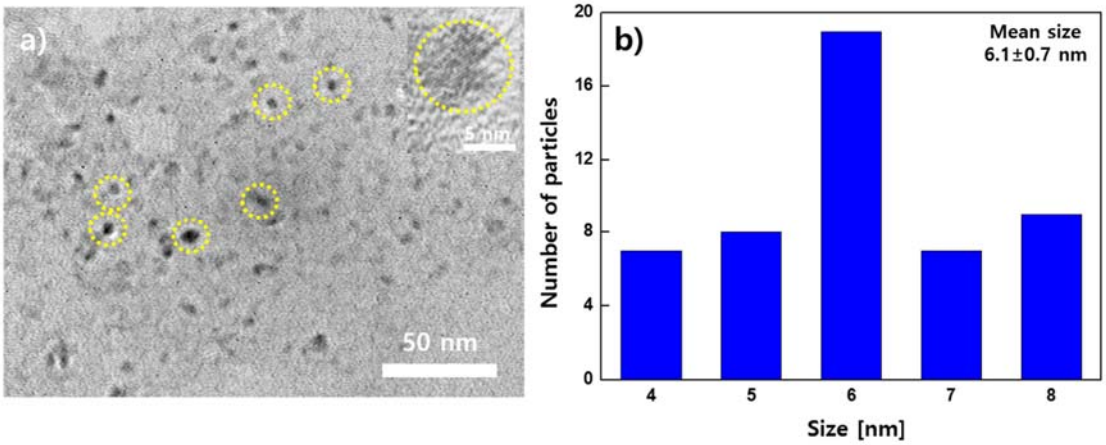

Figure 4.1. a) TEM image of NCDs and the inset show the HRTEM image and b) the corresponding particle size distribution.

Table 4.1. The atomic composition of the NCDs.

Sample	C [at.%]	H [at.%]	N [at.%]	O [at.%]
NCDs	54.89	28.66	12.43	4.03

The figure 4.2 (a) shows a XRD pattern of carbon dots. The broaden peak appeared at approximately 24° associated with C (002) and a small peak around 43° was indexed C (111). The result of XRD indicated that the NCDs consisted of intermediate a turbostratic structure contained graphite and amorphous structure together. Broad and low angle shift. The heteroatoms in the carbon structure lead to extend the distance between the layers. Thus, it caused a shift forward to a low angle. The result of Raman spectrum presented in figure 4.2 (b) shows that the D (1330 cm^{-1}) and G band (1550cm^{-1}) were observed. In detail, a defect of structure, disorder, and edge of carbon structure generate D band while the G band corresponds to the E_{2g} vibration in the plane of sp^2 carbon structure, as suggesting of graphitization degree [18]. Thus, the intensity ratio of two bands is commonly used for the amorphous degree of carbon material. The I_D/I_G ratio of NCDs (0.99) indicated that the hetero-atom in the carbon framework cause a degree of amorphous structure. For observation of functional groups on the NCDs surface, Fourier-transform infrared (FT-IR) spectroscopy was carried out and shown in the figure 4.2 (c). The broad absorption band related to OH and NH stretching was observed from 3680 to 3150 cm^{-1} [19, 20]. The existence of such bands contributes to making water-soluble NCDs. The band associated with sp^2 CH stretching was shown in 3072 cm^{-1} and sp^3 CH stretching of peaks were observed at 2919, and 2850 cm^{-1} [21]. The nitrile (C≡N) functional group also is clearly detected at 2200 cm^{-1}. The nitrile-functional group was formed by reaction with cyano radicals from the dissociation of the

pyridine molecule in plasma [16]. The band of vibration of stretching of aromatic C=C is confirmed at 1647 and 1504 cm^{-1}. The C-O and C=O band [22] were observed s from 1400 to 1200 cm^{-1}. It is considered that these functional groups related to oxygen were formed by OH from the plasma in water as mentioned before. The surface oxidation is significantly important for improving the quantum yield of the NCDs. The relationship between surface oxidation and quantum yield is described in detail in the part of fluorescence. The band related to the amino-functional group appeared in the range of 700-800 cm^{-1} [23]. It is reported that nitrile group molecule were formed in the pyridine due to dissociation by the SP. When the SP was generated in the pyridine and water mixture, the high concentration of hydrogen radicals from water molecules could lead to the conversion of nitrile-functional groups to amino-functional groups. The UV-VIS absorbance spectrum of the synthesized NCDs in the aqueous solution are presented in Fig. 4.2 (d). The typical absorption spectrum of colloidal the CDs solutions was shown π-π* transition band and another band indicating n-π* transition when the carbon dots contain heteroatoms [24]. All of the samples show the absorption peak of the π-π* transition at 250 nm. The broad shoulder bands centered at 330 nm related to n-π* transition bands were observed definitely.

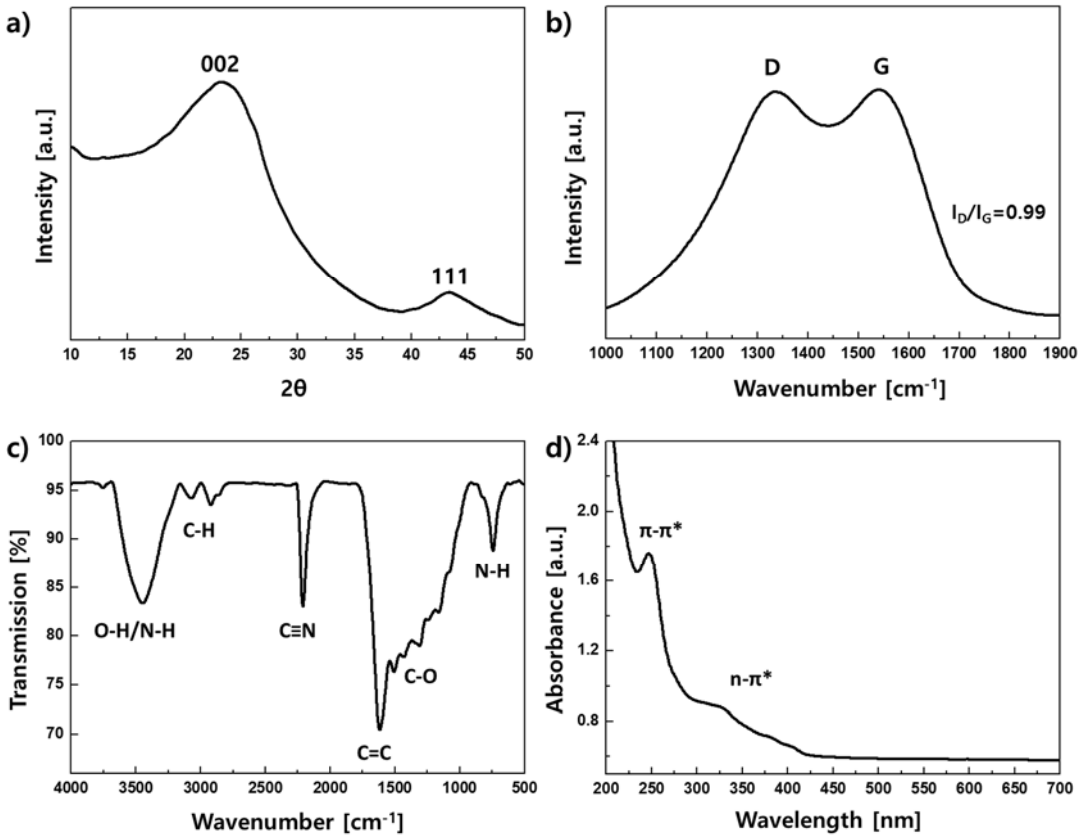

Figure 4.2. a) XRD pattern in the range of 20 to 80 degree, b) D and G band of NCDs in the Raman spectrum, c) Functional groups of NCDs in FT-IR spectrum and d) UV-vis absorption spectrum of NCDs dispersed in the water.

An overview of the chemical composition of the NCDs was obtained by XPS as Fig.4.3 a). In the wide range measurement, three peaks associated with C_{1s} (284.5 eV), N_{1s} (399.5 eV), and O_{1s} (532.5 eV) were observed in this spectrum. To confirm the nitrogen configuration, a high-resolution scan of N_{1s} was conducted as shown in figure.4.3 b). The spectra were deconvoluted into four peaks, pyridinic-N (399.0 ± 0.5eV), pyrrolic-N (400.0 ± 0.5eV), cationic-N (401.0 ± 0.5eV) and pyridinic-N oxide (402.5 eV). A representative scheme of N configuration was shown in figure.4.3 c). The N1s peak was contributed by N_P (42.2%), N_{Pr} (22.3%), N_C (29.6%), N_{Ox} (5.9%), respectively. In general, three kinds of N bonding configuration about the doped nitrogen atoms in 2D carbon strucutre, such as pyridinic N, pyrrolic N, and graphitic N (or quaternary N), are known generally. However, the N dopants can lead to deteriorating the planar structure due to their 5 valence electrons. For keeping the planar carbon structure, the cationic type of N dopant which has four valence electrons as same as carbon is suitable [25].

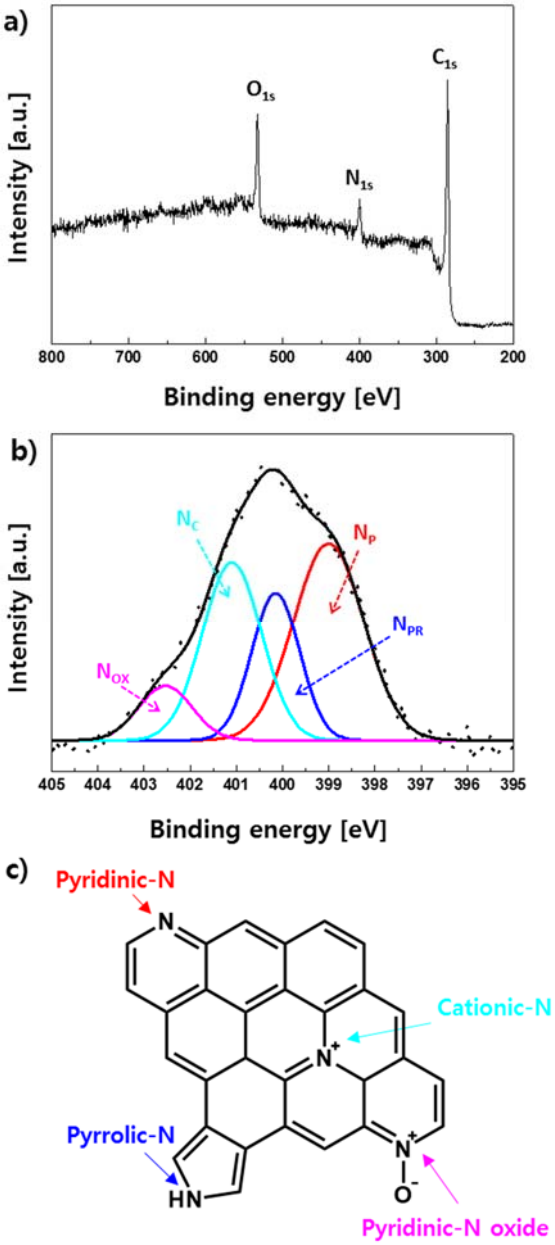

Figure 4.3. a) Wide range of XPS spectrum of NCDs, (b) high-resolution XPS N_{1s} spectrum of NCDs (N_P : pyridinic N, N_{PR} : pyrrolic N, N_C : cationic N, N_{OX} : oxidized N,), and c) Schematic representation of N atom configurations.

The figure.4.4 a) shows the NCDs solution in daylight and UV light and it showed that the NCDs solution emitted light blue fluorescence by excitation of the UV-light. To understand their fluorescence property, using different excitation wavelength, the fluorescence spectra (Fig. 4.4 b)) of NCDs were performed. The highest emission intensity was observed at 410 nm corresponding to 340 nm of excitation wavelength. The quantum yields of the NCDs were calculated by equation (1) with the standard molecule (Rhodamine B) and were found to be 61%. The value of parameters used in the calculation is presenting in table 4.2. In terms of energy efficiency, the quantum yield can be an important point of carbon dots. Generally, the quantum yield of carbon dots can be controlled by two factors, the presence of heteroatom and the surface passivation [26]. In this study, the nitrogen atom from the pyridine molecule is the heteroatom in the carbon structure. The lone pair electrons of nitrogen atoms generate n orbital as a HOMO level between existing π and π* orbital in the carbon structure. Therefore, the relatively narrow bandgap of n-π* transition, which is much closer to the range of visible light compared with that of π-π* transition, can emit the visible light efficiently by the excitation wavelength. In the case of our NCDs, the n-π* transition band was already confirmed in the range from 300 to 350 nm in the UV-vis result. Thus, the strong intensity fluorescence occur by the excitation wavelength in this range. Also, the surface passivation of the NCDs by oxygen atoms leads to the removal of dangling bonds in the structure. The presence of dangling bonds corresponded to numerous energy levels interfere with the excitation and recombination of electrons for fluorescence [27].

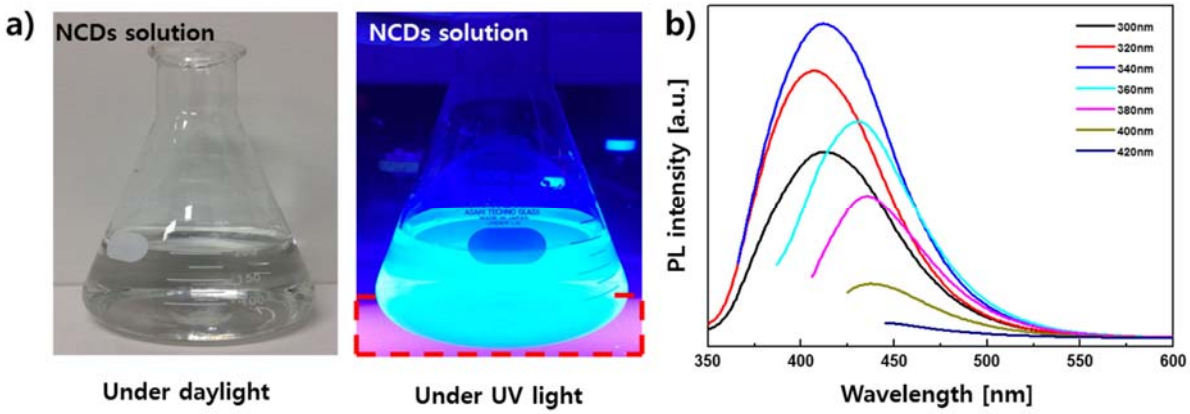

Figure 4.4. a) Comparasion of color on NCDs solution (20mg/200mL) under different kind of light and b) fluorescence spectra of NCD with different excitation wavelengths.

Table 4.2. The absorbance value (A) of UV-vis spectra at 340 nm, the integrated area (I) of emission under 340 nm, and quantum yield of the NCDs and Rhodamine-B.

Sample	Absorbance value (A)	Integrated area (I)	Quantum yield [%]
NCDs	0.82	76124	61
Rhodamine-B	0.27	12750	31

To reveal the detection property of TNP, the fluorescence response by adding various concentrations of TNP solutions were investigated under 340 nm of excitation wavelength. The fluorescence intensity of NCDs turned out to decrease obviously with 1μM of TNP and gradually decrease by concentration, as shown in figure 4.5(a). Finally, the peak of fluorescence almost disappeared when the TNP concentration is 500 μM. The quenching of the fluorescence depended on its concentration according to the Stern-Volmer equation.

$$F_0/F = 1 + K_{SV}C$$

Where F_0 and F mean fluorescence intensity with absence/presence of quenching molecules, respectively. The quenching constant and concentration of the quencher is given K_{SV} and C. Figure 4.5 b) represented the calibration graphs of the NCDs with a low concentration of the TNP. The quenching constant value (9.1×10^4 M^{-1}) and the LOD (10.1 nM) of the NCDs were obtain using the equation, respectively. The PET is one the fluorescence quenching mechanism that prohibits the emission due to the electron transfer from donor to acceptor. When the NCDs (donor) and TNP (acceptor) come close, the excited electron of the NCDs can transfer to the TNP, so the light emission of the NCDs do not occur. Thus, the efficiency of electron transfer could affect the sensitivity of the NCDs. The amino-functional group is a strong electron donor group among the functional groups, so it could enhance the efficiency of donating the excited electron from the NCDs. Consequentially, it was considered that the NCDs contained rich amino-functional group could detect the low concentration of TNP effectively. The quenching efficiency of the NCDs with other nitro groups molecules (NB, NN, NA, NF) was investigated to confirm the selectivity of the NCD for the TNP. As shown in figure 4.5 c), the quenching efficiency is 91% at 100 μM of the TNP, which is significantly higher than that of other molecules (NB : 0.1%, NN : 1.3%, NA : 2.9%, NF :

12%). Figure 4.5 d) also exhibited that only the TNP significantly weakened the fluorescence of the NCDs solution. The difference in the quenching efficiency between the NCDs and nitro group molecules came from the presence of hydroxyl groups. Because the hydroxyl groups of the TNP occurred the proton transfer assisted electron transfer with amino-functional groups on the surface of NCDs [28]. Therefore, the synergetic effect of the PET and the proton transfer assisted electron transfer could lead to the excellent selectivity of NCDs for TNP.

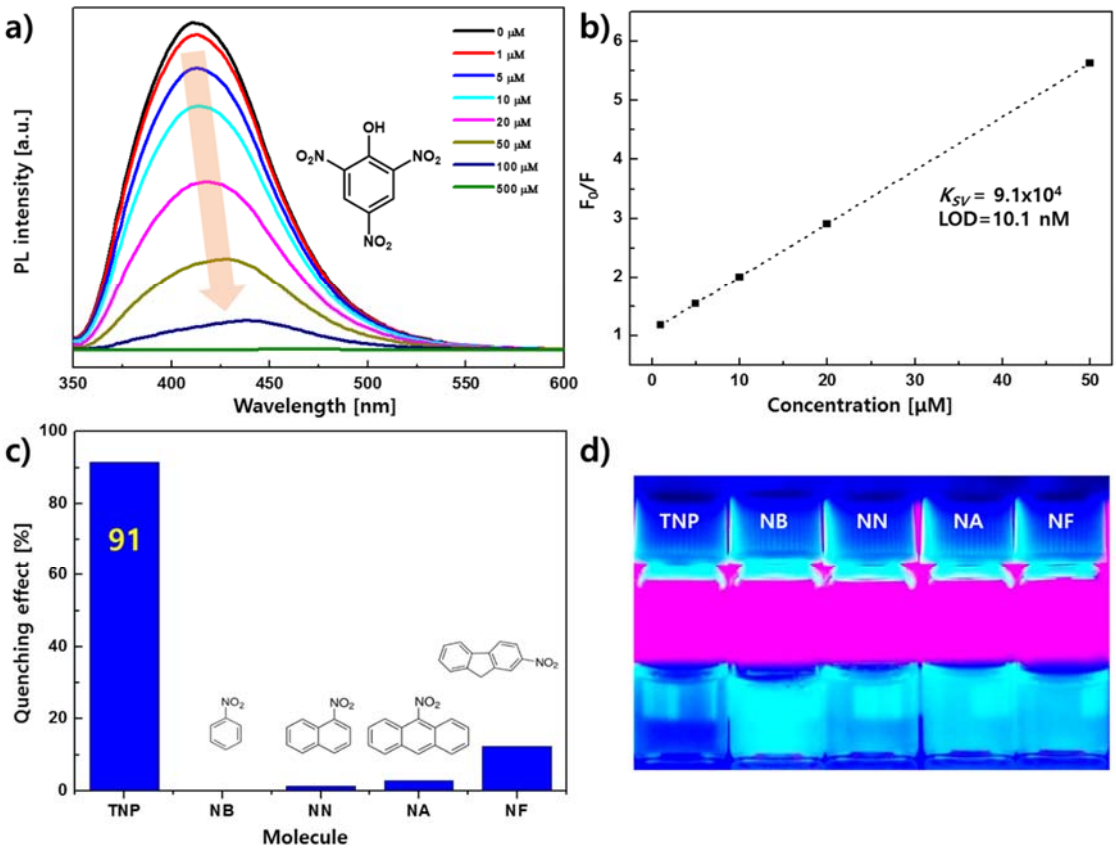

Figure 4.5. a) fluorescence spectra of NCD with different TNP concentration, b) F_0/F plot with the TNP low concentration region up to 50 μM, c) fluorescence quenching efficiency of the NCDs upon different nitro group molecules at 100 μM of concentration, and d) photograph of NCDs solutions mixed with different nitro group molecules under the UV light.

4.4. Summary

In conclusion, a strategy was established for the rapid synthesis of the NCDs with the amino-functional group through solution plasma for the effective detection of the TNP. The water-soluble NCDs have been successfully synthesized from pyridine and water for 10 minutes. The NCDs formed by pyridine and water mixture exhibited blue fluorescence with a high quantum yield (61%). This enhancement was due to the high N concentration and the surface passivation by radical from plasma. Meanwhile, as a TNP detector, the NCDs showed the highest sensitivity (LOD 10.1nM) due to their rich amino-functional groups as the pathway for electron transfer. Also, an excellent selectivity of the NCDs for the TNP was confirmed by a significantly high quenching efficiency at 91% as compared with the other nitro group molecules (0.1-12%).

References

1. E. Gaude, M.K. Nakhleh, S. Patassini, J. Boschmans, M. Allsworth, B. Boyle, M.P. van der Schee J. Breath. Res. 13 032001 (2019)

2. M. Norhayati, A. Bakar, A.A. Umar and J. G. Shapter, Advances in Natural Sciences 8 025008 (2017)

3. D. Shankaran, K. Gobi, N. Miura Sensor. Actuat. B-Chem. 121 158-177 (2007)

4. Z. Li, Y. Wang, Y. Ni, S. Kokot Spectrochim. Acta. A. Mol. Biomol. Spectrosc. 137 1213 (2015)

5. K.K. Chan, S.H.K. Yap, K.T. Yong Nanomicro. Lett. 10 72 (2018)

6. J. Shen, J. Zhang, Y. Zuo, L. Wang, X. Sun, J. Li, W. Han, R. He J. Hazard. Mater. 163 1199 (2009)

7. S. Zhu, Q. Meng, L. Wang, J. Zhang, Y. Song, H. Jin, K. Zhang, H. Sun, H. Wang, B. Yang Angew. Chem. Int. Ed. Engl. 52 3953 (2013)

8. X.T. Zheng, A. Ananthanarayanan, K.Q. Luo, P. Chen Small 11 1620 (2015)

9. X. Miao, D. Qu, D. Yang, B. Nie, Y. Zhao, H. Fan, Z. Sun Adv. Mater. 30 1704740 (2018)

10. D. Mandal, S. Khatun, A.N. Gupta, A. Chandra Nanotechnology 30 255501 (2019)

11. R. Cruz, P. Yro, G. Quiachon, C. Emolaga, M. Ysulat, U. Bigol and B. Basilia Mater. Sci. Eng. C 559 012003 (2019)

12. H. Li, W. Kong, J. Liu, N. Liu, H. Huang, Y. Liu, Z. Kang Carbon 91 66 (2015)

13. Q. Xu, P. Pu, J. Zhao, C. Dong, C. Gao, Y. Chen, J. Chen, Y. Liu, H. Zhou J. Mater. Chem. A 3 542 (2015)

14. J. Li, Y. Jiao, L. Feng, Y. Zhong, G. Zuo, A. Xie, W. Dong Microchim. Acta 184 2933 (2017)

15. N. Saito, M.A. Bratescu, K. Hashimi Jpn. J. Appl. Phys. 57 0102A4 (2018)

16. K. Kim, K. Hashimi, M.A. Bratescu, N. Saito Nanosci. Nanotech. Lett. 10 814 (2018)

17. I. Prasertsung, S. Kaewcharoen, K. Kunpinit, W. Yaowarat, N. Saito, T. Phenrat Water Sci. Technol. 79 967 (2019)

18. J.H. Kaufman, S. Metin, D.D. Saperstein S Phys. Rev. B. Condens. Matter 39 13053 (1989)

19. F.T. Ramanathan, R.S. Ruoff, and L.C. Brinson Chem. Mater. 17 6 (2005)

20. S.M. Yuen, C.M. Ma, Y.Y. Lin, H.C. Kuan Compos. Sci. Technol. 67 2564(2007)

21. H.G. Huang, J.Y. Huang, Y.S. Ning, G.Q. Xu J. Chem. Phys. 121 4820 (2004)

22. N.A. Travlou, D.A. Giannakoudakis, M. Algarra, A.M. Labella, E. Rodríguez-Castellón, T.J. Bandosz Carbon 135 104 (2018)

23. S. Tamilselvan, M. Vimalan, I.V. Potheher, S. Rajasekar, R. Jeyasekaran, M.A. Arockiaraj, J. Madhavan Spectrochim. Acta A Mol. Biomol. Spectrosc. 114 19 (2013)

24. K. Jiang, Y. Wang, X. Gao, C. Cai, H. Lin F Angew. Chem. Int. Ed. Engl. 57 6216 (2018)

25. S. Chae, G. Panomsuwan, M. Bratescu, K. Teshima, N. Saito ACS Appl. Nano Mater. 3 1350 (2019)

26. L. Li, T. Dong J. Mater. Chem. C 6 7944 (2018)

27. J.J. M. V. Wolkin, and P. M. Fauchet Phys. Rev. lett. 82 4 (1999)

28. B. JU, Y. Wang, Y. Zhang, T. Zhang, Z. Liu, M. Li, S. Zhang ACS Appl. Mater. Interface 10 13040 (2018)

Chapter 5

Summary

Chapter 5 – Summary

In the thesis, the investigation of a conversion of pyridine monomer by solution plasma was conducted. For synthesizing the hetero carbon nanomaterial, the new type of synthesizing method, solution plasma was employed. The solution plasma has a high potential to be an alternative method for simple and rapid synthesize nitrogen doped carbon nanomaterial with high nitrogen concentration. Thus, the researches on nitrogen doped carbon nanomaterial have been expanded with the solution plasma method. However, the fundamental study of hetero carbon nanomaterial fabricated by solution plasma is hardly proceeded yet. In particular, the synthesis pathway from the molecular level is still unrevealed. Therefore, an exploring of the conversion procedure from monomer to fabricating hetero carbon nanomaterial by SP is considered to have a worth to study.

In Chapter 1, the conventional synthesis methods of hetero carbon nanomaterials were introduced. The fundamental and experimental components of solution plasma as unconventional method were explained. The radical polymerization process was introduced to understand how the monomer be converted. At last, an introduction of the carbon dots which is nano scaled hetero carbon material was presented.

In Chapter 2, the initial reactions of pyridine for the synthesis of hetero-carbon nanomaterial by SP were presented. The pyridine solvents after SP 1 and 5 sec were analyzed by GC-MS. After a few seconds of SP, cyanopyridine, bipyridine, terpyridine, and phenanthroline molecules were formed. In the initiation step, CN, C_2, H radicals and pyridine cation radical

were generated in plasma phase and interface between plasma and liquid phase, respectively. In the propagation step, the CN and the pyridine cation radicals reacted with the pyridine molecules by the radical-nucleophilic aromatic substitution and CH activation, respectively. Finally, these radical polymerization reactions were finished by reaction with H and C_2 radicals. The results showed that from pyridine large molecules can be formed by radical reaction during solution plasma. Among the various kinds of products, 2,2'-bipyridine was confirmed to have the highest probability of synthesizing by density functional theory calculation.

In Chapter 3, we described a quantitative analysis of the molecules and radicals in the plasma phase using BAS method. To obtain the quantitative value, the integrated absorption band with transition oscillator strength. The number density of CN, C_2, H radicals during the SP in benzene, pyridine, and aniline were calculated, respectively. In the case of CN radical's number density, the value pyridine ($(1.1\pm0.7) \times 10^{16}$) is much higher than that of aniline ($(3.4\pm2.0) \times 10^{14}$). After SP, ten to hundred μM of arene and heteroarene were generated and were detected in the liquid. The products was formed by radicals from SP and the presence of phenyl radical in SP were explained by ESR measurement. At last, it is confirmed that SP has a potential for carbon nanomaterial synthesis as graphene and nitrogen-doped-graphene starting from arenes and heteroarenes by decreasing of H/C ratio.

In Chapter 4, we focused synthesis of carbon dots, few nanometers sized of carbon material through SP. A strategy for the synthesis of the nitrogen doped carbons dots which are previous step of common nitrogen doped black carbon was established. The idea based on that the pyridine can be polymerized to nanocarbon by the SP. Thus, we can control the size of hetero carbon nanomaterial with the condition change of the SP. At last, the water-soluble NCDs have been successfully synthesized from pyridine and water for 10 minutes. The prepared NCDs showed blue fluorescence with 61% of quantum yields. As a TNP detector, the NCDs showed

the highest sensitivity about 10 nM due to their rich amino-functional groups as the pathway for electron transfer. Also, an excellent selectivity of the NCDs for the TNP was revealed by an excellent high quenching efficiency at 91% as compared with the other nitro group molecules (0.1-12%).

In this study, various kinds of conversions from the pyridine monomer to dimer and trimer and several types of molecule by SP were successfully confirmed. Also, a fabricating to nitrogen doped carbon dots was confirmed. The results proved that SP methods can polymerize pyridine molecule rapidly and control the size of hetero carbon nanomaterial. Also, it suggested that suitable hetero carbon nano-material according to purpose can be synthesized by solution plasma. The pyridine as hetero arene is used in this study due to their similarity with benzene structure and their high synthesis rate of carbon nanomaterial. However, other types of hetero molecule also have a large potential to apply for synthesis of hetero carbon nanomaterial with prefer properties. Based on the results of this thesis, a pathway of other types of hetero molecule for hetero carbon nanomaterial will be discovered. Furthermore, it is believed that a molecular design by solution plasma can be achieved by revealing of the conversion procedure in molecular level of various kind molecules.

Achievement

List of publications

1. Kyusung Kim, Kazuo Hashimi, Maria Antoaneta Bratescu, and Nagahiro Saito*, "The Initial Reactions from Pyridine to Hetero-Carbon Nanomaterials through Solution Plasma", Nanoscience and Nanotechnology Letters, 10 (2018), 814-819.

2. Maria Antoaneta Bratescu, Kyusung Kim, and Nagahiro Saito*, "Quantitative spectrochemical analysis of solution plasma in aromatic molecules", Plasma Processes and Polymers, 16 (2019), e1900012

3. Kyusung Kim, and Nagahiro Saito*, "Rapid Synthesis of Highly N-doped Carbon Dots through Solution Plasma and their Molecular Detection Properties" submitted to Journal of nanoscience and nanotechnology

List of Reviews

1. 金奎成, 牟田幸浩, 橋見一生, Maria Antoaneta Bratescu, 齋藤永宏, ソリューションプラズマによるヘテログラフェンの合成と特性, 静電気学会誌, 42(3), (2018), 124-128.

List of awards

1. Outstanding Oral Presentation: Kyu-Sung Kim, Maria-Antoaneta Bratescu, and Nagahiro Satio, "Effect of N concentration in CQDs synthesized using Solution plasma", The 5th International Workshop on Solution Plasma and Molecular Technologies (SPM-5), MN-6, Cental hotel, Griefswald, Germany, (June 4 - 6, 2017).

2. Best Poster Rewards: Kyu-Sung Kim, Kazuo Hashimi, Maria-Antoaneta Bratescu, and Nagahiro Satio, "The Initial Reactions from Pyridine to Hetero-Carbon Nanomaterials through Solution Plasma", The 4th International Symposium on Hybrid Materials and Processing (Hymap 2017), PB-124-1191, Grand hotel, Busan, South Korea, (November 5 - 8, 2017).

3. 1st Oral Presentation: Kyu-Sung Kim, Maria-Antoaneta Bratescu, and Nagahiro Satio, “Nitrogen highly-doped Carbon dots Synthesized from Organic Monomer through Solution Plasma” The 6th International Workshop on Solution Plasma and Molecular Technologies (SPM-6), MN-03, Instutitue for Plasma science and technology, Gdansk, Poland, (June 4 - 6, 2018).

List of international presentation

- Oral presentation

1. Kyu-Sung Kim and Nagahiro Satio, “Investigation of N-doped Carbon Dots Synthesized by Solution Plasma for Detection of Nitro Aromatic Molecules”, The 5th edition of Nanotech France 2019 International Conference and Exhibition, IB-4-23, Palais des Congrès d'Issy Paris, France (June 26 - 28, 2019).

2. Kyu-Sung Kim, Maria-Antoaneta Bratescu, and Nagahiro Satio, “Nitrogen highly-doped Carbon dots Synthesized from Organic Monomer through Solution Plasma”, The 6th International Workshop on Solution Plasma and Molecular Technologies (SPM-6), MN-6, Cental hotel, Gdansk, Poland (June 4 - 6, 2018).

3. Kyu-Sung Kim, Maria-Antoaneta Bratescu, and Nagahiro Satio, “Investigation of initial reactions by solution plasma process in pyridine”, 2017 Workshop on Biomimetic Materials and Energy-saving Materials (2017 BMEM), Shanghai, China (November 24 - 26, 2017).

4. Kyu-Sung Kim, Maria-Antoaneta Bratescu, and Nagahiro Satio, “Effect of N concentration in CQDs synthesized using Solution plasma”, The 5th International Workshop on Solution Plasma and Molecular Technologies (SPM-5), MN-03, Instutitue for Plasma science and technology, Griefswald, Germany (June 4 - 6, 2017).

- Poster presentation

5. Kyu-Sung Kim, Jun-mo Moon and Nagahiro Satio, “Investigation of N-doped carbon dots synthesized by solution plasma for detecting nitro aromatic molecules”, AEPSE(Asian-European International Conference on Plasma Surface Engineering) 2019, S10-PO09, Maison glad hotel, Jeju, Korea (September 1 - 5, 2019).

6. Kyu-Sung Kim and Nagahiro Satio, “Enhancement of the Crystallinity of Nano-Carbon material

Synthesized by Solution Plasma", AEPSE(Asian-European International Conference on Plasma Surface Engineering) 2019, S10-PO10, Maison glad hotel, Jeju, Korea (September 1 - 5, 2019).

7. Kyu-Sung Kim, Maria-Antoaneta Bratescu, and Nagahiro Satio, "Synthesis of Highly Nitrogen-doped Carbon dots from organic monomer by solution plasma", The International Conference on Advanced and Applied Petroleum, Petrochemicals, and Polymers (ICAPPP2018), P-FPM-4, Chulalongkorn University, Bangkok, Thailand (December 18 - 20, 2018).

8. Kyu-Sung Kim, Maria-Antoaneta Bratescu, and Nagahiro Satio, "Synthesis of highly N-doped carbon dots through solution plasma for molecular detection", JSPS core to core Program Seminar, P-13, National University of Laos, Vientien, Laos (December 13-14, 2018).

9. Kyu-Sung Kim, Kazuo Hashimi, Maria-Antoaneta Bratescu, and Nagahiro Satio, "The Initial Reactions from Pyridine to Hetero-Carbon Nanomaterials through Solution Plasma", The 4th International Symposium on Hybrid Materials and Processing (HyMaP2017), PB-124-1191, Grand hotel, Busan, South Korea (November 5 - 8, 2017).

10. Kyu-Sung Kim, Maria-Antoaneta Bratescu, Oi Lun Helena Li and Nagahiro Satio, "Ultra High Sensitivity Attenuated Total Reflectance Based Ammonia Gas Sensor", 8th Nagoya Univ.-Tsinghua Univ.-Toyota Motor Corp.- Hokkaido Univ.-Xinjiang Normal Univ. Joint Symposium (8-NTTHX), S7-6, Xinjiang Normal University, Urumqi, China, (August 8 - 11, 2015)

List of domestic presentation

- Oral presentation

1. Kyu-Sung Kim and Nagahiro Satio, "Synthesis of N-doped carbon dot by solution plasma and its detection performance of nitro molecule", The Surface Finishing Society of Japan Meeting, 10E-03, Fukuoka Institute of Technology, Fukuoka, Japan (September 9 - 10, 2019).

2. Nagahiro Saito, Sang-Woo Chae, Kyu-Sung Kim, Yukihiro Muta, and Mongkol Tipplook, "Solution plasma and hetero graphene". Symposium on Biomimetic Materials Processing 2018 (BMMP-2018), Nagoya university, Nagoya, Japan (September 28 - 30, 2018).

3. Kyu-Sung Kim, Oi Lun Helena Li, Maria-Antoaneta Bratescu, and Nagahiro Satio, "Ultra High Sensitivity Attenuated Total Reflectance Based Ammonia Gas Sensor", D4-09-021, Yokohama Port

Opening Plaza, Yokohama, Japan (December, 8-10,2015)

4. Kyu-Sung Kim, Maria-Antoaneta Bratescu, Oi Lun Helena Li and Nagahiro Satio, “Develop of high sensitivity gas sensor using ATR method”, The Surface Finishing Society of Japan Meeting, 10A-28, Shinshu Unversity, Nagano, Japan (September 9 - 10, 2015).

- Poster presentation

5. Kyu-Sung Kim and Nagahiro Satio, “Synthesis of highly N doped carbon dots through solution plasma for molecular detection”, The 80th JSAP Autumn Meeting 2019 Surface Finishing Society of Japan Meeting, 21a-PB1-6, Hokkaido University, Hokkaido, Japan (September 9 - 10, 2019).

6. Kyu-Sung Kim, Maria-Antoaneta Bratescu, and Nagahiro Satio, “Effect of Nitrogen doping on the Fluorescence property of Carbon dots synthesized through Solution Plasma, The 79th Japan Society of Applied Physics (JSAP) Autumn Meeting, 18p-PB3-21, Nagoya Congress Center, Nagoya, Japan (September 18 - 21, 2018).

7. Kyu-Sung Kim, Kazuo Hashimi, Maria-Antoaneta Bratescu, and Nagahiro Satio, “Structural deformation of pyridine by solution plasma”, The Surface Finishing Society of Japan Meeting, P-90, Shibaura Institute of Technology, Tokyo, Japan (March 27 - 28, 2018).

8. Kyu-Sung Kim, Maria-Antoaneta Bratescu, and Nagahiro Satio, “Nitrogen highly-doped carbon dots synthesized from organic monomers by solution plasma”, Establishment of Research Hub for Compact Mobility Model in the ASEAN Region”, P-06, Nagoya University, Nagoya, Japan (February 27, 2018).